PHOTOSYNTHETIC PERFORMANCE OF TIDALLY FLOODED SPARTINA ALTERNIFLORA SALT MARSHES THROUGH FIELD MEASUREMENTS AND REMOTE SENSING PREDICTION

by

LISHEN MAO

(Under the Direction of Deepak R Mishra)

ABSTRACT

The photosynthetic performance of coastal marshes, an important blue carbon ecosystem, under tidal flooding has not been studied extensively. Our study aimed to understand coastal marsh plant photosynthesis at different stages of tidal inundation. Our study answered a few fundamental questions related to the differences in the photosynthesis rates between air-exposed and submerged parts of the canopy. We studied marsh Photosystem II (PSII) operating efficiency (φPSII) through a fundamental vegetation property called the chlorophyll fluorescence (ChlF) through, which can reflect the efficiency of marsh plants to utilize absorbed light energy to carry out photosynthesis. We designed and deployed a novel field measuring system that that measures high temporal resolution ChlF and φPSII at leaf scale. Our field observations demonstrated the within canopy variation of *Spartina alterniflora* ChlF and φPSII across a range of tidal cycles and differing tidal amplitudes. We also observed greatly reduced but active underwater photosynthesis activities in fully submerged leaves, suggesting that *S. alterniflora* potentially remains a carbon sink during tidal inundation. We further developed an integrated approach for parameterizing φPSII with a set of high-resolution environmental and biophysical measurements,

including air temperature (Tair), soil temperature (Tsoil), photosynthetically active radiation (PAR), tide height relative to the soil surface (WT), cloudiness index (CI), and the near-infrared reflectance of vegetation (NIRv). We incorporated these key meteorological and biophysical parameters into a random forest regression model to predict φPSII, which produced accurate results with a root mean square error of 0.9 (the observed φPSII ranges between 0.22 to 0.75). We also found that predicted *S. alterniflora* φPSII was predominantly driven by PAR, NIRv, Tsoil and WT. Our findings suggest that characteristics of salt marsh photosynthetic efficiency can be modelled by physiological and environmental variables. Our modeling revealed the seasonal and spatial variability of predicted φPSII over the Georgia Coastal Ecosystems Long Term Ecological Research (GCE-LTER) flux tower footprint. These findings will be beneficial in estimating salt marsh gross primary production (GPP). This novel framework can also be used as an important validation of ecosystem productivity models that rely on satellite data to study top of the canopy productivity.

INDEX WORDS: Chlorophyll Fluorescence; Leaf Level Photosynthesis; Photosystem II Working Efficiency; Random Forest Modeling; Pulse-Amplitude Modulation Fluorometry

PHOTOSYNTHETIC PERFORMANCE OF TIDALLY FLOODED SPARTINA ALTERNIFLORA SALT MARSHES THROUGH FIELD MEASUREMENTS AND REMOTE SENSING PREDICTION

by

LISHEN MAO

B.S., Eastern Michigan University, 2014

M.S., Eastern Michigan University, 2017

A Dissertation Submitted to the Graduate Faculty of The University of Georgia in Partial Fulfillment of the Requirements for the Degree

DOCTOR OF PHILOSOPHY

ATHENS, GEORGIA

2023

PHOTOSYNTHETIC PERFORMANCE OF TIDALLY FLOODED SPARTINA ALTERNIFLORA SALT MARSHES THROUGH FIELD MEASUREMENTS AND REMOTE SENSING PREDICTION

by

LISHEN MAO

Major Professor:	Deepak Mishra
Committee:	Marguerite Madden Lan Mu David Cotten Jessica O'Connell

Electronic Version Approved:

Ron Walcott
Vice Provost for Graduate Education and Dean of the Graduate School
The University of Georgia
May 2023

DEDICATION

I would like to dedicate this dissertation to my father Shuang Wang and my mother Xiaojiang Zeng. I have a reason because they are the best parent in the world. I also dedicate this dissertation to my girlfriend Wei Qian. I have a reason because she is the best girlfriend in the world. And for all the people who believed and helped me. This work would have never been completed without their supports.

TABLE OF CONTENTS

LIST OF TABLES

LIST OF FIGURES

LIST OF SYMBOLS

φPSII	PSII operating efficiency
BOC	Bottom of the *Spartina alterniflora* canopy
C	Carbon
ChlF	Chlorophyll fluorescence
CI	Cloudiness index
CO_2	Carbon dioxide
EC	Eddy covariance
ETR/rETR	Electron transport rate/relative electron transport rate
EVI	Enhanced vegetation index
F_0	Minimal fluorescence yield of leaf with maximal PSII centers open in the dark
F′	The steady-state level of fluorescence measured from leaf in the ambient actinic light
F_m	Maximal fluorescence yield of leaf with maximal PSII centers closed in the dark
F_m'	Maximal fluorescence yield of leaf with maximal PSII centers closed in the ambient actinic light
F_v	Variable fluorescence of leaf in the dark conditions, $F_m - F_0$
F_v/F_m	Maximum PSII operating efficiency
GAM	Generalized additive model

GCE LTER	Georgia Coastal Ecosystems Long Term Ecological Research
GPP	Gross primary productivity
LUE	Light use efficiency
MONI-DA	PAM fluorometry data acquisition logger
MONI-HEAD	PAM emitter-detector units
MONI – IB4/USB	PAM interface box for data communication
NEE	Net exchange of C between an ecosystem and the atmosphere
NDVI	Normalized difference vegetation index
NIR_V	Near-infrared reflectance of vegetation
NPQ	Non-photochemical quenching of fluorescence
OCO-2	Orbiting Carbon Observatory-2 satellite
PAM	Pulse amplitude modulation
PAR	Photosynthetically active radiation
PAR_{TOA}	Simulated PAR at the top of the atmosphere
PSII	Photosystem II, which yields variable fluorescence
PPFD	Photosynthetic photon flux density
PQ	Photochemical quenching of fluorescence
Q_A	Primary quinone acceptor of PSII
qL	Fraction of PSII reaction centers that are “open” for photochemistry
RMSE	Root mean squared error
S. alterniflora	*Spartina alterniflora*
SD	standard deviation

SIF	Solar induced fluorescence
Tair	Air temperature
Tsoil	Soil temperature
TOC	Top of the *Spartina alterniflora* canopy
WT	Tide height relative to the soil surface

Chapter 1:

INTRODUCTION

1.1. Background

Tidal marshes are among the most productive ecosystems and an important carbon (C) sink in the global C cycle (Bianchi, 2006). The average C burial rate of coastal salt marshes is as much as 1713 g C m^{-2} yr^{-1} in sediment, approximately 35 times higher than in terrestrial forests (McLeod *et al*., 2011). The C captured and stored in vegetated coastal ecosystems has been termed "blue carbon", it is also recognized as one of the most productive techniques to mitigate anthropogenic carbon dioxide (CO_2) emissions and defer global warming (NAS, 2019), which provides the key scientific motivation to understand salt marsh productivity across space and time. Salt marshes are vulnerable ecosystems with high dynamics of photosynthetic rate and plant production in the face of biophysical constrains such as high solar radiation and periodic tidal flooding (Hawman *et al*., 2021; Kathilankal *et al*., 2011; O'Connell *et al*., 2021). Pezeshki et al. (1993) showed that a congener, *Spartina patens*, had a 46% reduction in rates of photosynthesis and an 18% reduction in carbon assimilation under hypoxic (flooded) conditions in microcosm experiments. However, only a handful of studies have collected photosynthesis measurements at leaf level to understand the dynamics of photosynthetic behavior, particularly in an inter-tidal environment within tidal marshes (Duarte et al., 2005). Most studies used the CO_2 exchange between salt marshes and the atmosphere measured by eddy covariance (EC) systems to passively investigate tidal influences on marsh production at broad scales (Bonneville et al., 2008; Kathilankal et al., 2008; Moffett et al., 2010; Morris et al., 2013; Schäfer et al., 2014;

Artigas et al., 2015; Forbrich & Giblin, 2015; Nahrawi et al., 2020). For example, Kathilankal *et al*. (2008) demonstrated marsh–atmosphere C exchanges continued during mid-day flooding events in salt marshes dominated by the cosmopolitan marsh plant, *Spartina alterniflora*, Loisel (*S. alterniflora*) (Kartesz, 2015; USDA & NRCS, 2019) (= *Sporobolus alterniflorus*; Peterson *et al*., 2014a, 2014b), but leaf submergence suppressed *S. alterniflora* photosynthesis by 66% of that observed during high tides. The magnitude of the reduction of photosynthetic efficiency underwater may not be reflected directly in gas exchanges as Forbrich & Giblin (2015) found only small reductions (2-4%) in canopy level gas exchange from tidal inundation seasonal carbon budgets. The difference in the amount of tidal influence on C exchanges suggests that the EC carbon flux measurements are not able to accurately reflect leaf-scale dynamics in photosynthesis during tidal inundation because it essentially solves an inverse problem by measuring CO_2 fluxes to infer photosynthesis under tidal inundation. The reduction in canopy-scale CO_2 exchanges could likely be due to other factors such as laterally exported dissolved CO_2, low diffusion rates of CO_2 between the water column and atmosphere, or reduction in soil respiration by incoming tides (Kathilankal *et al*., 2008; Gålfalk *et al*., 2013). Therefore, more studies are needed to quantify leaf photosynthetic dynamics during different levels of plant submergence, to better understand and answer fundamental questions about the underlying energy partitioning mechanism of photosynthesis in flooded conditions, such as (a) do marsh canopies photosynthesize underwater? (b) if yes, what are their photosynthesis rates? (c) how does the photosynthesis rate vary between air-exposed and submerged parts of the canopy under different tidal flooding depths and during a specific tidal flooding cycle?

Active induced measurements of quantum yield of chlorophyll fluorescence (ChlF) with pulse amplitude modulated (PAM) fluorometry have a long history of research and been widely

exploited to study the acclimation of the photosynthetic apparatus at the leaf level for terrestrial biomes (Bilger *et al*., 1995; Porcar-Castell *et al*., 2008; Porcar-Castell, 2011; Maguire *et al*., 2020). For example, PAM fluorometry was utilized to evaluate the influence of intra-plant, inter-plants as well as environmental factors on photosynthetic activity in cocoa trees (Calzadillaet al., 2022). ChlF has been used as a key parameter in studying plant photosynthesis because it carries detailed information about the redox state of photosystem II (PSII) within chloroplasts (Murchie & Lawson, 2013). The underlying mechanism of using ChlF to study photosynthetic performance is straightforward. Light energy captured by chlorophyll in PSII undergoes three energy dissipation processes, often in combination, such that i) it can be used to drive photochemistry; ii) it can be lost from PSII as heat, or iii) it can be re-emitted from PSII as ChlF. Because these processes compete for the same light energy and PAM fluorometry is able to instantaneously inhibit the photochemistry of PSII (quenching of the fluorescence signal by plastoquinone reduction) by a high-intensity light pulse, the analysis of the leaf-level ChlF yield measured by PAM fluorometry provides direct, continuous information about changes in photochemical reactions such as nonphotochemical quenching (NPQ) resulting from changes in environmental variations. Therefore, long-term and continuous measurements of ChlF from the marsh leaf level can be used to investigate the complex dynamics of marsh photosynthetic activities via the estimated PSII operating efficiency (φPSII), particularly during tidal flooding in an inter-tidal environment. These data can also be coupled with environmental measurements to better understand the relationship between leaf photosynthesis and environmental gradients across different timescales and phenological stages.

Additional steps are required to scale the understanding of leaf level photosynthetic dynamics to larger areas for more comprehensive coverage of carbon exchange dynamics in

coastal ecosystems. A potential advancement in monitoring gross primary productivity (GPP, output from photosynthesis) would be to develop a product that captures the relationship between complex plant photosynthetic variability and the other environmental variables in coastal environments that can be eventually scaled up to larger areas and other tidal ecosystems. To our knowledge, such bottom-up models in a coastal salt marsh are sparse in the literature. Existing approaches in plant productivity monitoring are primarily focused on satellite-derived products with ground-level EC based net ecosystem exchange of CO_2 fluxes. For example, some studies exploited remote sensing of reflectance-based vegetation indices such as normalized difference vegetation index (NDVI) and enhanced vegetation index (EVI), and leveraged the temporal continuity of satellite-derived products to establish simple statistical relationships between remotely sensed vegetation indices and productivity (Churkina et al., 2005; D'Odorico et al., 2015; Fu et al., -2014; Rahman et al., 2005). These relationships have moderate explanatory power because they only capture overall changes in canopy structure and leaf pigments across time rather than canopy photosynthesis (Baker, 2008; Lee et al., 2013; Yang et al., 2018). Recent studies have started incorporating solar-induced fluorescence (SIF), a spectrum signal emitted by chlorophyll-a of assimilating plants after competing for absorbed light energy with photochemistry, to track the productivity variation at different spatial-temporal scales (Frankenberg et al., 2011; Guan et al., 2015; Joiner et al., 2013; Liu et al., 2017; Wen et al., 2020). Compared to reflectance-based vegetation indices, the passive SIF measurements are more directly linked with the physiological activities of the vegetation because they provide an indication of how much absorbed solar energy is used in photosynthesis in response to biophysical changes (Baker, 2008). Therefore, SIF, as an emerging technique, is playing an increasingly important role in evaluating plant responses to environmental changes as well as

improving carbon budget estimation (Qiu et al., 2018; Zhang et al., 2014). In the past several years, numerous studies have used SIF together with EC carbon fluxes measurements to study the seasonal variation of plant photosynthesis and the SIF-GPP relationship in different biomes and at different spatiotemporal scales, in which SIF signals were observed from towers (Yang et al., 2015), airborne (Damm et al., 2015) or satellite platforms (Bai et al., 2022). For example, Sun et al. (2017) found SIF retrieved from NASA's orbiting Carbon Observatory-2 (OCO-2) satellite was a reliable proxy for real time photosynthetic dynamics. They used the SIF-GPP relationship for three different biomes across space, including crops in Minnesota, grass at Stuart Plain in Australia, and deciduous temperate forests in Missouri. These measurements have already been successfully used in studies of crop productivity (Guanter et al., 2014; Guan et al., 2016) and drought monitoring (Yoshida et al., 2015; Sun et al., 2015) However, neither approach has been used to study photosynthesis in tidal marshes mainly due to the environmental constraints, in particular, tidal flooding and high solar radiation which tend to depress reflectance spectra and decouple SIF from photosynthesis function. These environmental heterogeneities caused by tidal dynamics increase the variability of the photosynthetic activity within coastal vegetation, introducing additional spatiotemporal complexities to the estimate of GPP. Therefore, developing a framework to model the responses of ChlF parameters (via PAM fluorescence) to environmental gradients commonly found in salt marsh environments is extremely valuable for understanding salt marsh photosynthetic activity at different spatial-temporal scales.

1.2. Objectives and Framework

The proposed research aims to leverage high frequency leaf-level ChlF measurements from PAM fluorometry and ground-based meteorological data to understand and quantify salt

marsh photosynthetic variations in the coastal intertidal ecosystem. An emphasis is placed on examining the impact of tidal flooding on the photosynthetic activities in salt marshes under natural field conditions. Additionally, this work focuses on developing a better understanding of the interactions between ChlF and environmental gradients. Specific objectives for this study include:

(1) To evaluate the practicality of using field-based PAM fluorometry for continuous measurements of ChlF in an intertidal salt marsh
(2) To study the variations in ChlF parameters and photosynthesis in *S. alterniflora* marshes under natural solar radiation and variable tidal flooding.
(3) To understand and quantify the influence of tidal inundation on *S. alterniflora* photosynthetic efficiency across canopy heights and tide ranges.
(4) To develop an accurate φPSII prediction model by linking biophysical and meteorological variables.
(5) To understand and quantify the environmental contributors of predicted φPSII by analyzing it with in-situ environmental parameters across different timescales and phenological stages.

References

Artigas, F., Shin, J. Y., Hobble, C., Marti-Donati, A., Schäfer, K. V. R., & Pechmann, I. (2015). Long term carbon storage potential and CO2 sink strength of a restored salt marsh in New Jersey. *Agricultural and Forest Meteorology, 200*, 313-321. doi:https://doi.org/10.1016/j.agrformet.2014.09.012

Baker, N. R. (2008). Chlorophyll Fluorescence: A Probe of Photosynthesis In Vivo. *Annual Review of Plant Biology, 59*(1), 89-113. doi:10.1146/annurev.arplant.59.032607.092759

Bai, J., Zhang, H., Sun, R., Li, X., Xiao, J., & Wang, Y. (2022). Estimation of global GPP from GOME-2 and OCO-2 SIF by considering the dynamic variations of GPP-SIF relationship. *Agricultural and Forest Meteorology, 326*, 109180.

Bianchi, T. S. (2006). *Biogeochemistry of Estuaries*. New York: Oxford University Press.

Bilger, W., Schreiber, U., & Bock, M. (1995). Determination of the quantum efficiency of photosystem II and of non-photochemical quenching of chlorophyll fluorescence in the field. *Oecologia, 102*(4), 425-432. doi:10.1007/BF00341354

Bonneville, M.-C., Strachan, I. B., Humphreys, E. R., & Roulet, N. T. (2008). Net ecosystem CO2 exchange in a temperate cattail marsh in relation to biophysical properties. *Agricultural and Forest Meteorology, 148*(1), 69-81. doi:https://doi.org/10.1016/j.agrformet.2007.09.004

Calzadilla, P. I., Carvalho, F. E. L., Gomez, R., Neto, M. L., & Signorelli, S. (2022). Assessing photosynthesis in plant systems: a cornerstone to aid in the selection of resistant and productive crops. Environmental and Experimental Botany, 104950.

Campbell, A. D., Fatoyinbo, L., Goldberg, L., & Lagomasino, D. (2022). Global hotspots of salt marsh change and carbon emissions. *Nature*, 1-6.

Churkina, G., Schimel, D., Braswell, B. H., & Xiao, X. (2005). Spatial analysis of growing season length control over net ecosystem exchange. *Global Change Biology, 11*(10), 1777-1787.

Damm, A., Guanter, L., Paul-Limoges, E., Van der Tol, C., Hueni, A., Buchmann, N., ... & Schaepman, M. E. (2015). Far-red sun-induced chlorophyll fluorescence shows ecosystem-specific relationships to gross primary production: An assessment based on observational and modeling approaches. *Remote Sensing of Environment, 166*, 91-105.

D'Odorico, P., Gonsamo, A., Gough, C. M., Bohrer, G., Morison, J., Wilkinson, M., ... & Buchmann, N. (2015). The match and mismatch between photosynthesis and land surface phenology of deciduous forests. *Agricultural and Forest Meteorology, 214*, 25-38.

Duarte, C. M., Middelburg, J. J., & Caraco, N. (2005). Major role of marine vegetation on the oceanic carbon cycle. *Biogeosciences, 2*(1), 1-8. doi:10.5194/bg-2-1-2005

Forbrich, I., & Giblin, A. E. (2015). Marsh-atmosphere CO2 exchange in a New England salt marsh. *Journal of Geophysical Research: Biogeosciences, 120*(9), 1825-1838. doi:https://doi.org/10.1002/2015JG003044

Frankenberg, C., Fisher, J. B., Worden, J., Badgley, G., Saatchi, S. S., Lee, J. E., ... & Yokota, T. (2011). New global observations of the terrestrial carbon cycle from GOSAT: Patterns of plant fluorescence with gross primary productivity. *Geophysical Research Letters*, *38*(17).

Fu, X., Tang, C., Zhang, X., Fu, J., & Jiang, D. (2014). An improved indicator of simulated grassland production based on MODIS NDVI and GPP data: A case study in the Sichuan province, China. *Ecological indicators*, *40*, 102-108.

Gålfalk, M., Bastviken, D., Fredriksson, S., & Arneborg, L. (2013). Determination of the piston

velocity for water-air interfaces using flux chambers, acoustic Doppler velocimetry, and IR imaging of the water surface. *Journal of Geophysical Research: Biogeosciences, 118*(2), 770-782. doi:https://doi.org/10.1002/jgrg.20064

Guan, K., Berry, J. A., Zhang, Y., Joiner, J., Guanter, L., Badgley, G., & Lobell, D. B. (2015). Improving the monitoring of crop productivity using spaceborne solar-induced fluorescence. *Global change biology*, *22*(2), 716-726.

Guanter, L., Zhang, Y., Jung, M., Joiner, J., Voigt, M., Berry, J. A., ... & Griffis, T. J. (2014). Global and time-resolved monitoring of crop photosynthesis with chlorophyll fluorescence. Proceedings of the National Academy of Sciences, 111(14), E1327-E1333.

Hawman, P. A., Mishra, D. R., O'Connell, J. L., Cotten, D. L., Narron, C. R., & Mao, L. (2021). Salt Marsh Light Use Efficiency is Driven by Environmental Gradients and Species-Specific Physiology and Morphology. *Journal of Geophysical Research: Biogeosciences*, *126*(5), e2020JG006213. doi:https://doi.org/10.1029/2020JG006213

Kartesz, J. T. (2015). The biota of North America program (BONAP). *North American plant atlas*, *412*, 413.

Kathilankal, J. C., Mozdzer, T. J., Fuentes, J. D., D'Odorico, P., McGlathery, K. J., & Zieman, J. C. (2008). Tidal influences on carbon assimilation by a salt marsh. *Environmental Research Letters, 3*(4), 044010. doi:10.1088/1748-9326/3/4/044010

Kathilankal, J. C., Mozdzer, T. J., Fuentes, J. D., McGlathery, K. J., D'Odorico, P., & Zieman, J. C. (2011). Physiological responses of Spartina alterniflora to varying environmental conditions in Virginia marshes. *Hydrobiologia, 669*(1), 167. doi:10.1007/s10750-011-0681-9

Lee, J. E., Frankenberg, C., van der Tol, C., Berry, J. A., Guanter, L., Boyce, C. K., ... & Saatchi,

S. (2013). Forest productivity and water stress in Amazonia: Observations from GOSAT chlorophyll fluorescence. Proceedings of the Royal Society B: Biological Sciences, 280(1761), 20130171.

Liu, L., Guan, L., & Liu, X. (2017). Directly estimating diurnal changes in GPP for C3 and C4 crops using far-red sun-induced chlorophyll fluorescence. *Agricultural and Forest Meteorology*, *232*, 1-9.

Joiner, J., Guanter, L., Lindstrot, R., Voigt, M., Vasilkov, A. P., Middleton, E. M., ... & Frankenberg, C. (2013). Global monitoring of terrestrial chlorophyll fluorescence from moderate-spectral-resolution near-infrared satellite measurements: methodology, simulations, and application to GOME-2. *Atmospheric Measurement Techniques*, *6*(10), 2803-2823.

Maguire, A. J., Eitel, J. U. H., Griffin, K. L., Magney, T. S., Long, R. A., Vierling, L. A., . . . Bruner, S. G. (2020). On the Functional Relationship Between Fluorescence and Photochemical Yields in Complex Evergreen Needleleaf Canopies. *Geophysical Research Letters*, *47*(9), e2020GL087858. doi:https://doi.org/10.1029/2020GL087858

Mcleod, E., Chmura, G. L., Bouillon, S., Salm, R., Björk, M., Duarte, C. M., ... & Silliman, B. R. (2011). A blueprint for blue carbon: toward an improved understanding of the role of vegetated coastal habitats in sequestering CO2. *Frontiers in Ecology and the Environment*, *9*(10), 552-560.

Moffett, K. B., Wolf, A., Berry, J. A., & Gorelick, S. M. (2010). Salt marsh–atmosphere exchange of energy, water vapor, and carbon dioxide: Effects of tidal flooding and biophysical controls. *Water Resources Research*, *46*(10). doi:https://doi.org/10.1029/2009WR009041

Morris, J., Sundberg, K., & Hopkinson, C. (2013). Salt Marsh Primary Production and Its Responses to Relative Sea Level and Nutrients in Estuaries at Plum Island, Massachusetts, and North Inlet, South Carolina, USA. *Oceanography, 26*, 78-84. doi:10.5670/oceanog.2013.48

Murchie, E. H., & Lawson, T. (2013). Chlorophyll fluorescence analysis: a guide to good practice and understanding some new applications. *Journal of Experimental Botany, 64*(13), 3983-3998. doi:10.1093/jxb/ert208

Nahrawi, H., Leclerc, M. Y., Pennings, S., Zhang, G., Singh, N., & Pahari, R. (2020). Impact of tidal inundation on the net ecosystem exchange in daytime conditions in a salt marsh. *Agricultural and Forest Meteorology, 294*, 108133.

NAS, 2019. Negative Emissions Technologies and Reliable Sequestration: A Research Agenda

O'Connell, J. L., Mishra, D. R., Alber, M., & Byrd, K. B. (2021). BERM: a Belowground Ecosystem Resiliency Model for estimating Spartina alterniflora belowground biomass. *New Phytologist, 232*(1), 425-439. doi:https://doi.org/10.1111/nph.17607

Peterson, P. M., Romaschenko, K., Arrieta, Y. H., & Saarela, J. M. (2014). (2332) Proposal to conserve the name Sporobolus against Spartina, Crypsis, Ponceletia, and Heleochloa (Poaceae: Chloridoideae: Sporobolinae). *TAXON, 63*(6), 1373-1374. doi:https://doi.org/10.12705/636.23

Peterson, P. M., Romaschenko, K., Arrieta, Y. H., & Saarela, J. M. (2014). A molecular phylogeny and new subgeneric classification of Sporobolus (Poaceae: Chloridoideae: Sporobolinae). *TAXON, 63*(6), 1212-1243. doi:https://doi.org/10.12705/636.19

Pezeshki, S. R., Pardue, J. H., & Delaune, R. D. (1993). The influence of soil oxygen deficiency on alcohol dehydrogenase activity, root porosity, ethylene production and photosynthesis

in Spartina patens. *Environmental and Experimental Botany, 33*(4), 565-573. doi:https://doi.org/10.1016/0098-8472(93)90031-A

Porcar-Castell, A. (2011). A high-resolution portrait of the annual dynamics of photochemical and non-photochemical quenching in needles of Pinus sylvestris. *Physiologia Plantarum, 143*(2), 139-153. doi:https://doi.org/10.1111/j.1399-3054.2011.01488.x

Porcar-Castell, A., Pfündel, E., Korhonen, J. F. J., & Juurola, E. (2008). A new monitoring PAM fluorometer (MONI-PAM) to study the short- and long-term acclimation of photosystem II in field conditions. *Photosynthesis research, 96*(2), 173-179. doi:10.1007/s11120-008-9292-3

Qiu, B., Xue, Y., Fisher, J. B., Guo, W., Berry, J. A., & Zhang, Y. (2018). Satellite chlorophyll fluorescence and soil moisture observations lead to advances in the predictive understanding of global terrestrial coupled carbon-water cycles. Global Biogeochemical Cycles, 32(3), 360-375.

Rahman, A. F., Sims, D. A., Cordova, V. D., & El-Masri, B. Z. (2005). Potential of MODIS EVI and surface temperature for directly estimating per-pixel ecosystem C fluxes. *Geophysical Research Letters, 32*(19).

Schäfer, K. V. R., Tripathee, R., Artigas, F., Morin, T. H., & Bohrer, G. (2014). Carbon dioxide fluxes of an urban tidal marsh in the Hudson-Raritan estuary. *Journal of Geophysical Research: Biogeosciences, 119*(11), 2065-2081. doi:https://doi.org/10.1002/2014JG002703

Sun, Y., Frankenberg, C., Wood, J. D., Schimel, D. S., Jung, M., Guanter, L., ... & Yuen, K. (2017). OCO-2 advances photosynthesis observation from space via solar-induced chlorophyll fluorescence. Science, 358(6360), eaam5747.

Sun, Y., Fu, R., Dickinson, R., Joiner, J., Frankenberg, C., Gu, L., ... & Fernando, N. (2015). Drought onset mechanisms revealed by satellite solar-induced chlorophyll fluorescence: Insights from two contrasting extreme events. *Journal of Geophysical Research: Biogeosciences*, *120*(11), 2427-2440.

USDA, N. (2019). The PLANTS Database. Greensboro, NC: National Plant Data Team. In.

Wen, J., Köhler, P., Duveiller, G., Parazoo, N. C., Magney, T. S., Hooker, G., ... & Sun, Y. (2020). A framework for harmonizing multiple satellite instruments to generate a long-term global high spatial-resolution solar-induced chlorophyll fluorescence (SIF). *Remote Sensing of Environment*, *239*, 111644.

Yang, K., Ryu, Y., Dechant, B., Berry, J. A., Hwang, Y., Jiang, C., ... & Yang, X. (2018). Sun-induced chlorophyll fluorescence is more strongly related to absorbed light than to photosynthesis at half-hourly resolution in a rice paddy. Remote Sensing of Environment, 216, 658-673.

Yang, X., Tang, J., Mustard, J. F., Lee, J. E., Rossini, M., Joiner, J., ... & Richardson, A. D. (2015). Solar-induced chlorophyll fluorescence that correlates with canopy photosynthesis on diurnal and seasonal scales in a temperate deciduous forest. *Geophysical Research Letters*, *42*(8), 2977-2987.

Yoshida, Y., Joiner, J., Tucker, C., Berry, J., Lee, J. E., Walker, G., ... & Wang, Y. (2015). The 2010 Russian drought impact on satellite measurements of solar-induced chlorophyll fluorescence: Insights from modeling and comparisons with parameters derived from satellite reflectances. *Remote Sensing of Environment*, *166*, 163-177.

Zhang, Y., Guanter, L., Berry, J. A., Joiner, J., van der Tol, C., Huete, A., ... & Köhler, P. (2014). Estimation of vegetation photosynthetic capacity from space-based measurements of

chlorophyll fluorescence for terrestrial biosphere models. Global change biology, 20(12), 3727-3742.

Chapter 2:

STUDY SITE

2.1. Overall Description of Study Site

Our study was conducted on the coast of Georgia on Sapelo Island within the Georgia Coastal Ecosystems Long Term Ecological Research (GCE LTER) site (Figure 2.1). Sapelo Island is a state-protected barrier island that contains over 40 ha of salt marsh dominated by a monoculture of *S. alterniflora* (Bortolus *et al*., 2019). We focused on *S. alterniflora* because it is the most common salt marsh plant along the southeastern coast of the United States (Ainouche *et al*., 2003), and is further found on all three coasts of the conterminous United States and nearly every continent globally as either a native or invasive species. Thus, a better understanding of *S. alterniflora* photosynthesis dynamics is important because of its broad spatial coverage. Further, other common marsh plants also grow in monoculture, such as *Spartina patens* and *Juncus roemerianus*, two other species that are widespread on the southeastern coast of the United States (Gleason & Zieman, 1981; Smart, 1982), and which respond to similar ecological drivers. Thus, our *S. alterniflora* study is the first step toward understanding more broadly salt marsh photosynthesis dynamics in field settings. Our study sites consisted of marsh complexes within Keenan Field and near the Sapelo Island Flux, both along the eastern side of Duplin River (Figure 2.2a). The linear distance between these two sites is approximately 660 m. Both marshes experienced similar meteorological conditions but differed in canopy morphology (plant height).

Figure 2.1 The overall location of Sapelo island on the east coast of Georgia, U.S.A. Background imagery is a Landsat satellite images by Earthstar, from 2023-01-12.

2.2. Experimental Sites

We deployed the PAM fluorometry at the Keenan Field marsh site at Latitude 31.444° and Longitude −81.283° (Figure 2.2b). *S. alterniflora* in this area varies in height along an elevation gradient, with tall-form plants (> 100 cm) along the low elevation creekbank, medium (50 to 100 cm), and short-forms (< 50 cm) in intermediate and high marshes, respectively. Tall form plants are the most typical plants in this area (O'Connell *et al*., 2019). Our field data were collected from July 11, 2020 to July 27, 2020, in the marsh interior at a tall- to medium-form

ecotone, approximately 25 m east of the Duplin River, and ~8 m north of the nearest tidal creek. Mean stem heights of our study plants were 110 ± 2.3 cm. The elevation of this study location averaged 72 cm NAVD88 based on centimeter-accurate in-situ RTK measurements, which is an intermediate marsh elevation in this area, where elevation ranged from 20 cm to 110 cm (Alber & O'Connell, 2019).

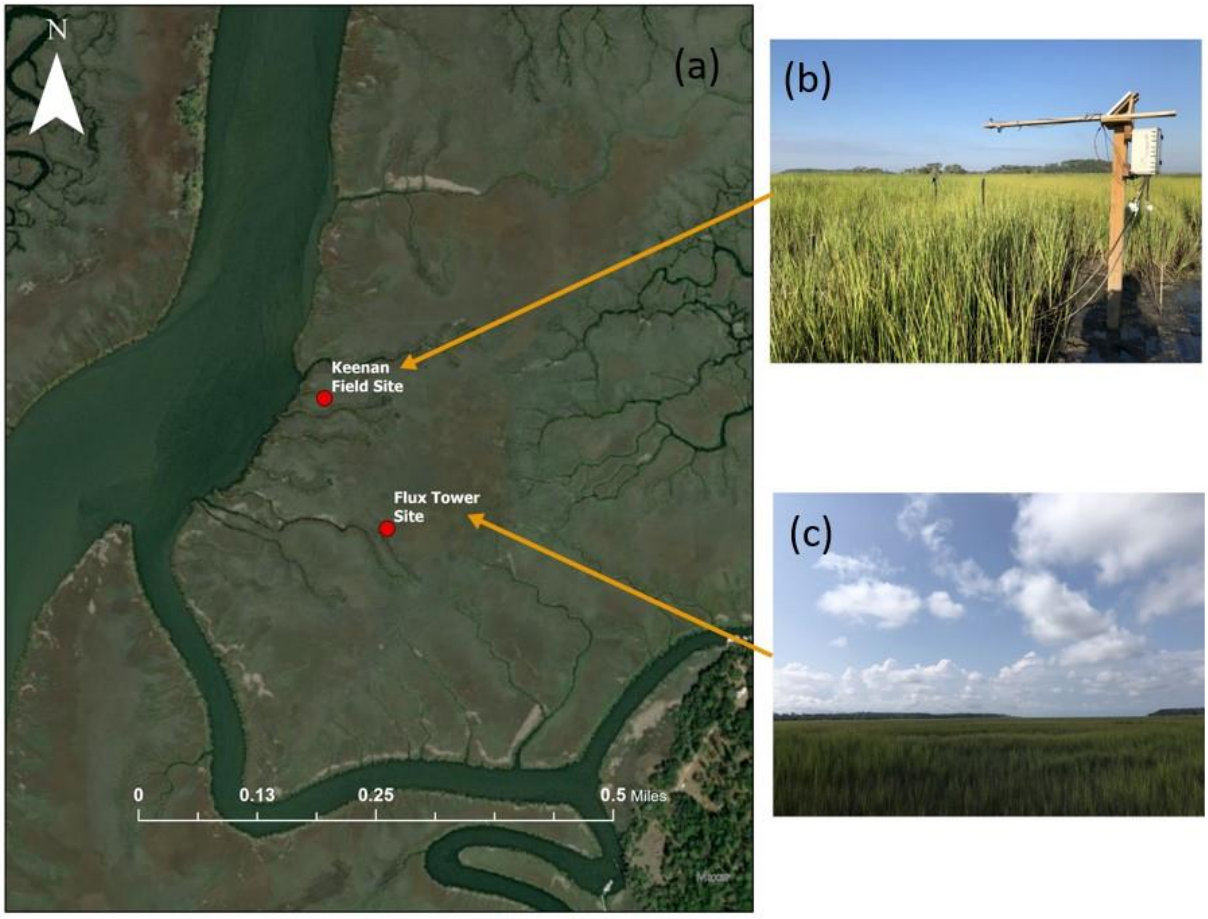

Figure 2.2 Field data collections in our study came from two Spartina alterniflora salt marshes sites on Sapelo Island, Georgia, USA. (a) Locations of the observation instruments (red dots) used for the Chlorophyll fluorescence (ChlF) and meteorological measurements, and photos of the vegetation at (b) Keenan Field site in the marsh interior at a tall- to medium-form ecotone

taken on July 10, 2020, (c) Flux tower marshes site adjacent to an eddy covariance carbon flux tower taken on August 22, 2018.

The Flux tower site was near the GCE-LTER EC carbon flux tower at Latitude 31.444° and Longitude −81.283°, approximately 245 m east of the Duplin River (Figure 2.2c). This site had similar elevations as the Keenan Field PAM deployment location, but Keenan Field site is situated on a tidal creek natural levy, while the flux tower site is on the interior and higher elevation marsh platform. Medium-form *S. alterniflora* dominated this region with 71.3 ± 13 cm mean canopy height during our sampling between August 22, 2018, and September 10, 2018. High tides occur twice daily with typical tidal heights from 0 to 60 cm over the marsh platform (Hawman *et al*., 2021), but not high enough to completely inundate the marsh platform. During the majority of tidal inundation, *S. alterniflora* at both sites were only partially submerged, and leaves at the top of the canopy were exposed to the atmosphere. Neither site experienced disturbance (e.g., hurricane, dieback, wrack deposition) during our sampling period.

Reference

Ainouche, M. L., Baumel, A., Salmon, A., & Yannic, G. (2003). Hybridization, polyploidy and speciation in Spartina (Poaceae). *New Phytologist, 161*(1), 165-172. Doi:https://doi.org/10.1046/j.1469-8137.2003.00926.x

Alber, M., & O'Connell, J. L. (2019). Elevation Drives Gradients in Surface Soil Temperature Within Salt Marshes. *Geophysical Research Letters, 46*(10), 5313-5322. Doi:https://doi.org/10.1029/2019GL082374

Bortolus, A., Adam, P., Adams, J. B., Ainouche, M. L., Ayres, D., Bertness, M. D., ... & Weis, J. S. (2019). Supporting *Spartina*: Interdisciplinary perspective shows *Spartina* as a distinct solid genus. Ecology 100:e02863. Doi.org/10.1002/ecy.2863

Gleason, M. L., & Zieman, J. C. (1981). Influence of tidal inundation on internal oxygen supply of Spartina alterniflora and Spartina patens. *Estuarine, Coastal and Shelf Science, 13*(1), 47-57. Doi:https://doi.org/10.1016/S0302-3524(81)80104-1

Hawman, P. A., Mishra, D. R., O'Connell, J. L., Cotten, D. L., Narron, C. R., & Mao, L. (2021). Salt Marsh Light Use Efficiency is Driven by Environmental Gradients and Species-Specific Physiology and Morphology. *Journal of Geophysical Research: Biogeosciences, 126*(5), e2020JG006213. doi:https://doi.org/10.1029/2020JG006213

O'Connell, J. L., Alber, M., & Pennings, S. C. (2019). Microspatial Differences in Soil Temperature Cause Phenology Change on Par with Long-Term Climate Warming in Salt Marshes. *Ecosystems, 23*(3), 498-510. doi:10.1007/s10021-019-00418-1

Smart, R. M. (1982). Distribution and environmental control of productivity and growth form of Spartina alterniflora (Loisel.). In D. N. Sen & K. S. Rajpurohit (Eds.), *Contributions to the ecology of halophytes* (pp. 127-142). Dordrecht: Springer Netherlands.

Chapter 3:

METHODOLOGY

3.1. Leaf-scale Chlorophyll Fluorescence Measurements

We used the aquatic version of a Monitoring PAM chlorophyll fluorometry to measure leaf-level ChlF (Heinz Walz GmbH, Effeltrich, Germany). The aquatic Monitoring PAM fluorometry consists of one data acquisition logger (MONI – DA), one PC interface box (MONI – IB4/USB), and four emitter-detector units (MONI – HEAD). They are connected using waterproof data communication cables (RS – 485). A built-in battery and 500 Megabytes microSD card are sealed within MONI – DA/S, which allows for consistent monitoring of ChlF under frequent flooding conditions (water resistance up to 75 m). MONI – HEAD is a compact (~250 g) 3-cm wide by 28-cm long water-tight aluminum cylinder with built-in photosynthetically active radiation (PAR) and temperature sensors. It also has a blue LED light (peak at 455 nm) that is used to deliver measuring light, actinic light, as well as a saturating pulse, which is situated within a sample clip for modulated fluorescence measurements. The leaf clip was mounted at a distance of 2.5 cm and 120º from the lens.


Moni-DA
Plant Monitoring System
MONI
RESET
MEM.
ON
OFF
SAT
ESC
MENU

(a)

(b)


WALZ
Model: Moni-IB1/S
S/N: CFMIJ0114
Made in Germany

(c)

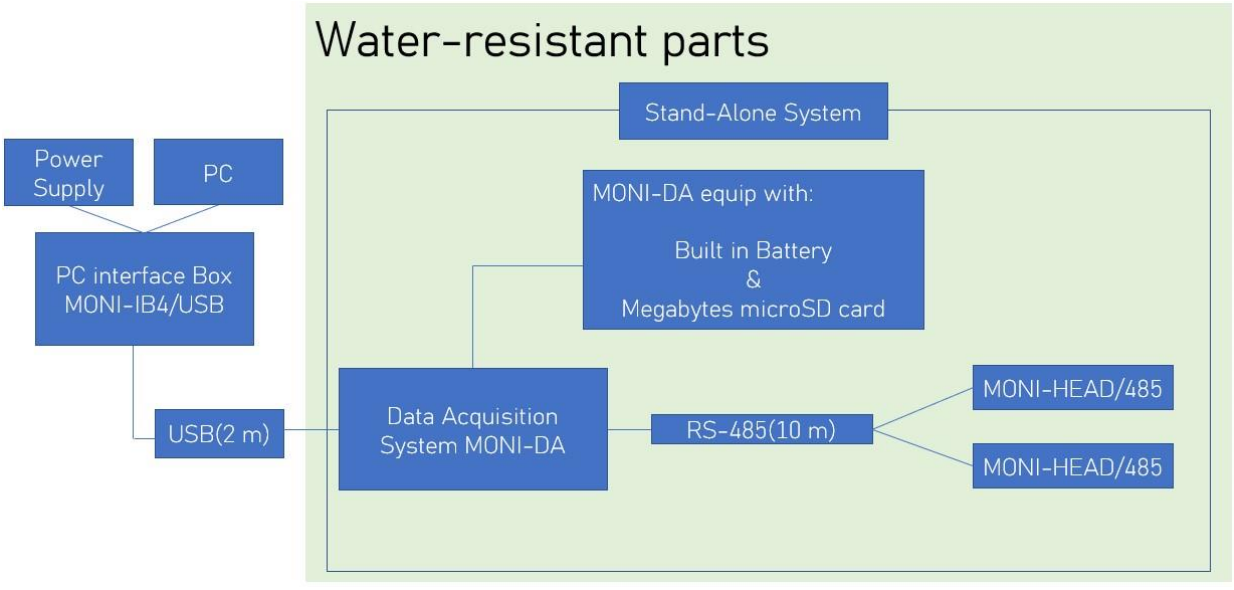
Water-resistant parts
Stand-Alone System
Power Supply
PC
PC interface Box MONI-IB4/USB
MONI-DA equip with:
Built in Battery
&
Megabytes microSD card
USB(2 m)
Data Acquisition System MONI-DA
RS-485(10 m)
MONI-HEAD/485
MONI-HEAD/485

(d)

Figure 3.1 Multi-Channel PAM Chlorophyll Fluorometry system (a) MONI-DA Data Acquisition system with 4 MONI-HEAD measuring head on the side, (b) Standalone MONI-HEAD measuring head with sample clip consisting of 2 plastic frames, (c) MONI- IB4/USB PC Interface box that is used as a battery charger for MONI-DA and for data communication, (d) Example system configuration for ChlF data collection in the field.

We inserted two to three pairs of green and healthy *S. alterniflora* leaves into each sample clip because a single *S. alterniflora* leaf, particularly at the top of the canopy, was not wide enough to cover the entire clip. We also placed a black high-density foam behind the sample clip to eliminate background interference (Figure 3.2). In addition, we added Polyurethane foam at the top and bottom edges of the clip holder to ensure that leaves remained in place through tidal inundation (Figure 3.2). It also reduced the etiolation symptoms of leaves throughout the monitoring period. The intensity of measuring light at the sample clip level is adjustable, ranging from 0.1 $\mu mol \cdot m^{-2} \cdot s^{-1}$ at low frequency (5 Hz) to 15 $\mu mol \cdot m^{-2} \cdot s^{-1}$ at high frequency (500 Hz). The same blue LED emits up to 1,500 $\mu mol \cdot m^{-2} \cdot s^{-1}$ actinic light and up to 2s saturation pulse for a maximally 6,000 $\mu mol \cdot m^{-2} \cdot s^{-1}$ at the sample clip level. A filter is used within the lens of MONI – HEAD to exclusively isolate the reflected ChlF signal at wavelengths > 645 nm.

Figure 3.2 a detailed view of the MONI – HEAD measuring head in the field with three *S. alterniflora* leaves selected in the sampler clip.

In order to ensure robust ChlF measurements during tidal inundation, we built a rectangular PVC frame from 1-inch PVC pipes for MONI – HEAD deployment (Figure 3.3a). Each corner of the rectangular base was secured to the soil by a PVC leg (screwed to the frame and inserted into the soil 60 cm). The two long sides of the base were connected by a PVC pipe (80 cm in length). From the middle of this connector, a central PVC pipe (110 cm in length) rose vertically from the center position of the rectangular base, creating a stable mount for the sensor (Figure 3.3b).

(a)

(b)

Figure 3.3 Pictures of custom-made PVC frame that supports ChlF measurements from *S. alterniflora* plant (a) lab picture of our PVC frame, (b) field picture of our PVC frame.

We used two MONI – HEAD to measure the tidal influences on ChlF of *S. alterniflora* at two different stem heights: one each at the top of the canopy (TOC) and bottom of the canopy (BOC), approximately 105 and 35 cm from the soil surface. MONI-HEAD/S were installed on the custom-made PVC frames (Figure 3.4). The position of the top sensor was determined by the marsh plant height (average canopy height was 110 ± 2.3 cm during sampling). The bottom sensor position was determined by the height of the leaves lowest on the plant stem.

Figure 3.4 Field picture of leaf-level ChlF measurement system that installed on a custom-made PVC frame that supports ChlF measurements from *S. alterniflora* at the top and bottom of the plant canopy

ChlF parameters, including maximum ChlF in dark (F_m) and in light (F_m'), minimal ChlF in dark (F_0), and steady-state fluorescence (F') were measured by each MONI- HEAD. The intensity of the measuring light was set as 0.1 $mol \cdot m^{-2} \cdot s^{-1}$ under "low-frequency" mode in dark and 15 $\mu mol \cdot m^{-2} \cdot s^{-1}$ under "high-frequency" model in light, respectively. The saturation light used maximum Photosynthetic Photon Flux Density (PPFD) with 0.8s integration time. The measuring light switched off after each saturating measurement but automatically switched on before the next saturating pulse. *S. alterniflora* leaves were sampled at 5 minutes intervals,

resulting in 288 data points collected daily, which allowed us to continuously monitor the influence of tides on *S. alterniflora* photosynthetic activities. The final 2020 dataset included 4,896 observations from each MONI-HEAD, with 9,792 observations in total. The final 2018 dataset had 3792 observations, which added up to a total of 10,000 data points at 5 min intervals over the sampling period across two years.

3.2. Leaf-scale Chlorophyll Fluorescence Measurements

All measured and derived ChlF parameters are listed in Table 3.1 and described below.

Table 3.1 Description of chlorophyll fluorescence parameters used in this study.

Parameter	**Definition**	**Measurement**
F_0	Minimal fluorescence measured from a leaf in the dark	Measured after dark-adapted leaf exposed to weak measuring light
F_m	Maximum fluorescence measured from a leaf in the dark	Measured after dark-adapted leaf exposed to saturating light pulse
F_v	Range in leaf fluorescence during dark conditions	Difference in fluorescence between F_m and F_0: $F_v = F_m - F_0$
F_v/F_m	Maximum quantum efficiency of PSII; the range in fluorescence vs. maximal fluorescence during dark conditions	Proportion of fluorescence: F_v/F_m
F'	The steady-state level of fluorescence measured from leaf in the ambient actinic light. Sometimes referred to as F_t in the literature	Measured under ambient light conditions before any saturating light pulse

F_m'	Maximum leaf fluorescence measured in the ambient actinic light	Measured under ambient light after the leaf is exposed to saturating light pulse
F_q'	Range in leaf fluorescence from in actinic light	Difference in fluorescence between F_m' and F': $F_q' = F_m' - F'$
φPSII	PSII operating efficiency: the proportion of light absorbed by PSII that is used for photosynthesis	Proportion of fluorescence between F_q' and F_m': F_q' / F_m'

Note: The parameter with a prime (') notation represents measurements from the leaf under continuous actinic light that drives photosynthesis. The parameter without a prime represents continuous measurements from the leaf in the dark, where modulated measuring light absorbed by PSII is used completely for photochemistry.

Fluorescence measurement provides leaf-level information on the acclimation of PSII energy partitioning in a natural environment (Adams & Demming-Adams, 2004; Logan *et al*., 2007; Baker, 2008). The F_0 and F_m were measured in the dark-adapted state (i.e., pre-dawn). The maximum quantum yield of PSII (F_v/F_m) was calculated following Maxwell & Johnson (2000) as:

$$F_v/F_m = (F_m-F_0) / F_m$$

Where, F_v/F_m indicates the maximal photosynthetic potential of a dark-adapted leaf with no heat dissipation and all reaction centers open.

PSII operating efficiency (φPSII) is the fluorescence parameter that indicates the efficiency at which light is absorbed by PSII. φPSII is used for a light-adapted leaf and estimates photochemistry yield. φPSII was determined following Genty *et al*. (1989) as:

$$\varphi PSII = (F_m' - F') / F_m'$$

Where, F_m' is the fluorescence maximum in the light-adapted state, and F' is the fluorescence yield at which the absorbed radiant energy is emitted from the *S. alterniflora* leaf in actinic light conditions. Theoretically, F' is higher than F_0 as the primary quinone acceptor (Q_A) cannot become maximally oxidized (i.e., PSII reaction centers are not completely open) in light environments (Baker, 2008). In addition, F_m' should be lower than F_m because of an increase in the efficiency of heat dissipation (i.e., non-photochemical quenching- NPQ) with increasing light intensity (Murchie & Lawson, 2013).

3.3. Leaf-scale Photosynthetic Photon Flux Density (PPFD) Measurements

In order to carefully examine the impact of tidal inundation on the photosynthetic dynamics of salt marshes, we continuously measured the incident PAR that plants received at different stem heights under natural field conditions. We used LI-192 (LI-COR Biosciences, Lincoln, NE), an underwater quantum sensor that is accurate in air and underwater. To minimize reflectance interference from the instrument frame, upwelling and downwelling quantum sensors were fixed on a black finished metal frame (LICOR 2009S lowering frame), and then mounted on black painted PVC pipes (1-inch diameter PVC pipes, henceforth expressed as 'PAR tree'; Figure 3.5). During 2020 sampling, two PAR trees were deployed to simultaneously measure downwelling PAR at different stem heights of the plant (at 105 cm and 35 cm from the soil surface, respectively), which corresponds to the heights of the TOC and BOC PAM measurements described previously (Figure 3.5a, b). The PAR acquisition frequency was programmed to match PAM ChlF data. We then used a waterproof cable (LI-COR 2222UWB) to transmit PaR to a XLite 9210B data logger (Sutron Corporation, Sterling, VA) (Figure 3.5c). In 2018 sampling, we measured the incident PAR on the flux tower using LI-190R (LI-COR

Biosciences, Lincoln, NE, USA) quantum sensor. Sensor readings were also automatically logged every 5 min by a Campbell Scientifics CR3000 data logger on the flux tower (Figure 3.7).

(a)

(b)

(c)

Figure 3.5 Field deployment of LI-192 quantum sensor at different levels of canopy. (a) a set of LI-192 quantum sensors measured upwelling and downwelling PAR at the top of the marsh with the help of the customized frame. (b) a set of LI-192 quantum sensors measured upwelling and downwelling PAR at the bottom of the marsh with the help of the customized frame. (c) a solar

panel powered XLite 9210B data logger (Sutron Corporation, Sterling, VA) that connected to sets of LI-192 quantum sensors and automatically recorded solar radiation measurements.

We calibrated the PPFD data obtained from underwater quantum sensors (LI-192) for both in-air and underwater conditions. The photon intensity at different plant heights was determined following the factory LI-192 calibration equation: Radiation = Measured Current × Calibration Multiplier. Where, the measured current was the output of the sensor in microamps, and the calibration multiplier was a multiplier that distinguishes sensor operating conditions. For example, an underwater multiplier is always greater than an in-air multiplier because of the immersion effect. We applied an immersion coefficient multiplier to the BOC quantum sensor when it was fully submerged. In this context, we post-calibrated 2186 downwelling measurements from the quantum sensor at BOC with the corresponding tide height and immersion coefficient multiplier. We did not apply an underwater multiplier to the TOC measurements because it was never submerged during the sampling.

3.4. Tide Height Measurements

We used HOBO U20 Water Level Data Logger (Onset Computer Corporation, Bourne, MA) to record water table heights near the PAM fluorometers at Keenan Field in 2020 (Figure 3.6a). These water table measurements were taken ~4.8 m east of MONI – HEAD at an elevation of 0.76 m NAVD88. We placed the sensor in a well (2-inch diameter PVC pipe) that was 39 cm above the vegetated marsh soil surface. We drilled infiltration holes every 20 cm on four sides of the pvc well to stimulate groundwater flow. We also used a fabric cloth as a cover to prevent sedimentation (Figure 3.6c). The HOBO logger was programmed to collect well water level data in 5-minute intervals, concurrent with ChlF measurements. We calculated the water table height relative to the soil surface (WT) for MONI – HEAD and ‘PAR trees’ by subtracting

the soil surface elevation at the sensor location from the water height. Thus, positive values represent water levels above the soil surface. 2018 water table measurements were measured at a creek ~ 50 m southeast of the flux tower at 31.4437° and -81.2838° with an elevation of 0.7 m NAVD88 using Campbell CS456 titanium pressure transducer (Campbell Scientific Inc., Logan, UT, USA) (Figure 3.6b). This system has been maintained by GCE-LTER field technicians. Sensor readings are automatically logged by a Campbell Scientifics CR3000 data logger on the flux tower (Figure 3.7) and were converted to those relative to the soil surface as well. This allowed for direct comparison in tide level during flooding between the two sites despite differences in marsh soil surface elevation.

(a)

(b)

(c)

Figure 3.6 Picture and field deployment of pressure transducer sensor. (a) HOBO U20 Water Level Data Logger, (b) Campbell CS 456 Titanium Pressure Transducer (c) A customized PVC well with fabric cover and infiltration holes built to secure Hobo U20 data logger for continuous water height measurements caused by tidal inundation.

3.5. Plant submergence status definition

To determine the influence of tidal inundation on the photosynthetic performance of *S. alterniflora*, we designated three conditions of tidal inundation from the BOC perspective, including fully submerged, partially submerged, and air-exposed. In our study, air-exposed indicates leaves that are exposed to the atmosphere. Fully submerged indicates conditions when the BOC leaves are completely submerged. Partially submerged represents conditions when leaves at the height of BOC sensor are exposed to the atmosphere, but plants below the BOC sensor are fully submerged. This is a transient period for plants between getting submerged with the rising tide (tide moves in) and being exposed with the receding tide (tide moves out). TOC leaves were always exposed to the air during our sampling period. We also focused on mid-day flooding that peaked between 10:00 and 16:00 US EST following Kathilankal et al. (2008).

3.6. Cloudiness Index

We also calculate cloudiness Index (CI) to represent the variation of sky conditions. The index of cloudiness is created based on the relationship between observed and potential PAR at the top of the atmosphere. The CI calculation following Turner et al. (2003) and Turner et al. (2006):

$$\mathrm{CI} = 1 - \mathrm{PAR}/\mathrm{PAR}_{TOA} \quad (1)$$

where PAR is the incident PAR measured at the canopy $\mathrm{PAR}_{\mathrm{TOA}}$ is the simulated PAR at the top of the atmosphere (following Hawman et al. 2021). The CI value is in the range of 0-1, with a lower value indicating a higher percentage of clouds in the sky (e.g., overcast), and a higher value representing clear conditions with fewer clouds in the sky (e.g., sunny)

3.7. Air temperature data

To identify meteorology conditions for this study, we obtained 5-min air temperature (Tair) data from the flux tower for the sampling periods. The air temperature measurements were taken at two different elevations of the flux tower (Figure 3.7) by three different sensors, including the 107 thermocouple (Campbell Scientific Inc., Logan, UT, USA) at the top of the tower and two separate sensors HMP45C (Campbell Scientific Inc., Logan, UT, USA) and EE181 (Campbell Scientific Inc., Logan, UT, USA) at the middle level of the tower. We used averages of temperature measurements made at different locations in our study.

3.8. Soil temperature data

The GCE EC flux tower also has soil temperature (Tsoil) sensors that collect information at 5-min intervals. Soil temperatures were taken at a depth integrated between 5 - 10 cm. We used Tsoil measurements from the EC flux tower for the Keenan filed in 2020 because the elevation gradients between these two sites were small (~0.3 m), which we hypothesize might not lead to significant differences in soil temperature across the study marsh. A separate temperature probe (HOBO UA-002, Onset Computer Corporation, Bourne, MA) buried into the soil to measure soil temperature will be included in the future study.

3.9. The near-infrared reflectance of vegetation (NIR_V) index

In addition to above mentioned environmental variables, we calculated near-infrared reflectance of vegetation (NIR_V) from the Sentinel-2 remote sensing satellite. The NIR_V is calculated as the product of NIR reflectance and the normalized difference vegetation index (NDVI) following Badgley et al., 2017. NDVI is a common measure of vegetation cover, but it is not a good proxy for intertidal salt marshes as the tidal inundation can significantly impact the reflectance of the canopy, resulting in a decrease in the NDVI sensitivity and accuracy. NIR

reflectance should be a more robust proxy of leaf photosynthetically active radiation (fPAR) absorbed by a canopy as well as canopy chlorophyll content (Dechant et al., 2022) because it is more attributable to vegetation phenology (Sellers et al., 1992). We calculated the NIR_V to match our sampling period between August 22 and September 10, 2018, and from July 11 to July 27, 2020, using 45 Sentinel-2 images/dates. We first selected dates without flooding by applying FLATS index to our Sentinel images (Narron et al., 2022). Then we used Smoothing Spline Regression in R to interpolate 28 days of dry Sentinel-2 images between June 13, 2018 and Jan 28, 2021 to the entire sampling period.

Figure 3.7 GCE-LTER flux tower with sensor positions marked with numbers. The positions of interest to our study are #1: air temperature sensor at the top of the tower (107 thermocouple);

#2: air temperature sensor at mid-tower (HMP45C); #3: newer air temperature sensor at mid-tower (EE181)

3.10. Random Forest modeling

We used the random forest model (Liaw, Wiener, et al., 2002), a commonly used algorithm in classification and regression, to model the relationship between φPSII and environmental variables. We used a fast implementation of random forests (Ranger) (Breiman 2001), from the *R* package "randomForest". Random forest model is among the types of models that could be used for regression analysis when the input data have high spatial and temporal variabilities. It also allows for nonlinear modeling between the dependent and independent variables without a prior assumption of underlying relationships. In the random forest algorithm, hundreds of decision trees are randomly generated, and all trees are independent of each other. A final regression model is the most accurate with respect to predicting ground-truth information and made by aggregating multiple layers of the decision trees. In this study, a random forest model was trained for φPSII data with the above-mentioned environmental covariates (Eq. 2). The final formula for this study was:

$$\varphi PSII \sim f\{Tair, Tsoil, WT, PAR, CI, NIR_V\} \quad (2)$$

We first divide our data into global training and global validation sets. The global training set included data collected in August 2018 from the flux tower site and July 2020 from the Keenan field site; the global validation set has comprised of data collected in September 2018 (09/01/2018 – 09/10/2018). These two datasets were independent, and in particular, the global validation data were collected at a different timeframe and was expected to reduce the overfitting in model evaluation.

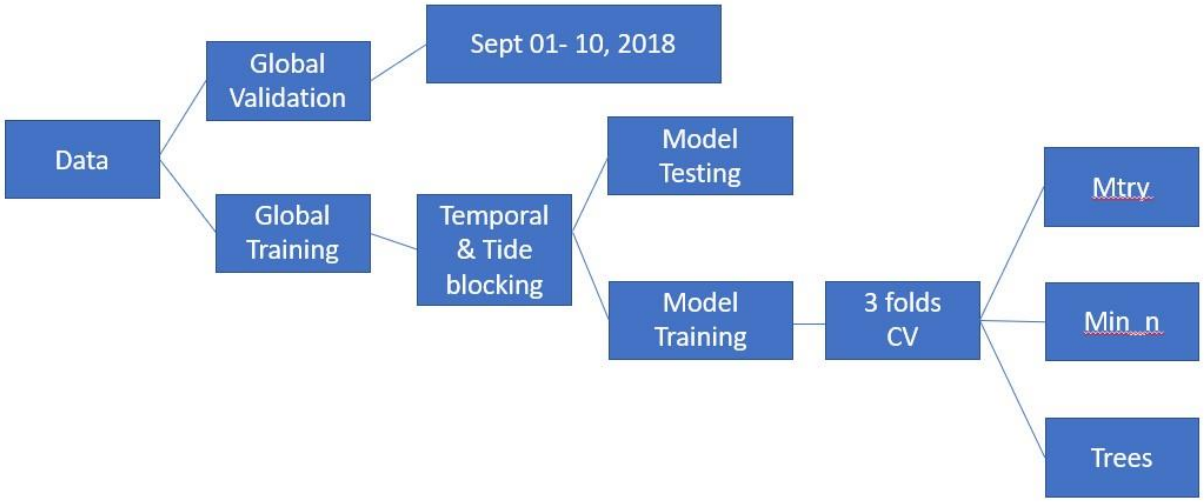

Figure 3.8 Full schema of random forest model training, testing and validation datasets set up.

Second, we created the model resampling based on the global training data from the last step. We divided the global training dataset into a model training and testing set (70% and 30% of the global training data, respectively). We used this 70/30 relationship because empirical studies have shown that it could produce the best results and avoid overfitting (Gholamy et al., 2018). To account for temporal autocorrelation within closely observed samples and prevent overfitting and overly optimistic model accuracy, we used a procedure known as temporal blocking (Meyer et al., 2018). This involved keeping observations from the same day together during the splitting process. In addition, we stratified the splitting by tidal flooding (tide blocking) to ensure that model training and testing sets contained observations from different tidal conditions and were thus more representative of the entire dataset.

Third, random forest model results can be different based on the choices of model parameters. In order to find the best performing parameters for our model, we used "Hyperparameter tuning" and "Cross-Validation". Hyperparameter tuning is a method where one

optimizes the parameter within the training set during random forest model building. The model resampling was used to tune the model hyperparameters on the model training dataset and validated on the model testing dataset via repeated 3-fold cross-validation with the number of repeating = 10. To select hyperparameters, we used an optimization via a regularized grid search across three parameters, including (1) trees - number of trees in the forest, (2) min_n - minimum number of samples allowed within the terminal node, and (3) mtry - the number of variables to consider for splitting a node. We selected the best-performing parameters in the tuning results based on the root mean squared error (RMSE), fit the finalized random forest model to the global training, and evaluated it on the global testing dataset. At last, we calculated the default variable importance output of the random forest model for each predictor using the *R* package “vip”.

Reference

Adams, W. W., & Demmig-Adams, B. (2004). Chlorophyll Fluorescence as a Tool to Monitor Plant Response to the Environment. In G. C. Papageorgiou & Govindjee (Eds.), *Chlorophyll a Fluorescence: A Signature of Photosynthesis* (pp. 583-604). Dordrecht: Springer Netherlands.

Badgley, G., Field, C. B., & Berry, J. A. (2017). Canopy near-infrared reflectance and terrestrial photosynthesis. *Science advances*, *3*(3), e1602244.

Baker, N. R. (2008). Chlorophyll Fluorescence: A Probe of Photosynthesis In Vivo. *Annual Review of Plant Biology*, *59*(1), 89-113. doi:10.1146/annurev.arplant.59.032607.092759

Bischl B, Mersmann O, Trautmann H, Weihs C. 2012. Resampling methods for meta-model validation with recommendations for evolutionary computation. *Evolutionary Computation* **20**: 249– 275.

Breiman, L. Random Forests. *Machine Learning* **45**, 5–32 (2001). https://doi.org/10.1023/A:1010933404324

Dechant, B., Ryu, Y., Badgley, G., Köhler, P., Rascher, U., Migliavacca, M., ... & Berry, J. A. (2022). NIRVP: A robust structural proxy for sun-induced chlorophyll fluorescence and photosynthesis across scales. *Remote Sensing of Environment*, *268*, 112763.

Elias, S. P., Gardner, A. M., Maasch, K. A., Birkel, S. D., Anderson, N. T., Rand, P. W., et al. (2020). A generalized additive model correlating blacklegged ticks with white-tailed deer density, temperature, and humidity in Maine, USA, 1990–2013. Journal of Medical Entomology, 58(1), 125–138. https://doi.org/10.1093/jme/tjaa180

Genty, B., Briantais, J.-M., & Baker, N. R. (1989). The relationship between the quantum yield of photosynthetic electron transport and quenching of chlorophyll fluorescence.

Biochimica et Biophysica Acta (BBA) - General Subjects, 990(1), 87-92. doi:https://doi.org/10.1016/S0304-4165(89)80016-9

Gholamy, A., Kreinovich, V., & Kosheleva, O. (2018). Why 70/30 or 80/20 relation between training and testing sets: A pedagogical explanation.

Hawman, P. A., Mishra, D. R., O'Connell, J. L., Cotten, D. L., Narron, C. R., & Mao, L. (2021). Salt Marsh Light Use Efficiency is Driven by Environmental Gradients and Species-Specific Physiology and Morphology. *Journal of Geophysical Research: Biogeosciences, 126*(5), e2020JG006213. doi:https://doi.org/10.1029/2020JG006213

Hyndman, R. J., & Koehler, A. B. (2006). Another look at measures of forecast accuracy. *International journal of forecasting, 22*(4), 679-688.

Liaw, A., & Wiener, M. (2002). Classification and regression by randomForest. *R news, 2*(3), 18-22.

Kathilankal, J. C., Mozdzer, T. J., Fuentes, J. D., D'Odorico, P., McGlathery, K. J., & Zieman, J. C. (2008). Tidal influences on carbon assimilation by a salt marsh. *Environmental Research Letters, 3*(4), 044010. doi:10.1088/1748-9326/3/4/044010

Logan, B., Adams, W., & Demmig-Adams, B. (2007). Viewpoint: Avoiding common pitfalls of chlorophyll fluorescence analysis under field conditions. *Functional Plant Biology - FUNCT PLANT BIOL, 34*. doi:10.1071/FP07113

Maxwell, K., & Johnson, G. N. (2000). Chlorophyll fluorescence—a practical guide. *Journal of experimental botany, 51*(345), 659-668

Meyer, H., Reudenbach, C., Hengl, T., Katurji, M., & Nauss, T. (2018). Improving performance of spatio-temporal machine learning models using forward feature selection and target-oriented validation. *Environmental Modelling & Software, 101*, 1-9.

Murchie, E. H., & Lawson, T. (2013). Chlorophyll fluorescence analysis: a guide to good practice and understanding some new applications. *Journal of Experimental Botany, 64*(13), 3983-3998. doi:10.1093/jxb/ert208

Narron, C. R., O'Connell, J. L., Mishra, D. R., Cotten, D. L., Hawman, P. A., & Mao, L. (2022). Flooding in Landsat across Tidal Systems (FLATS): An index for intermittent tidal filtering and frequency detection in salt marsh environments. *Ecological Indicators*, *141*, 109045.

Sellers, P. J., Berry, J. A., Collatz, G. J., Field, C. B., & Hall, F. G. (1992). Canopy reflectance, photosynthesis, and transpiration. III. A reanalysis using improved leaf models and a new canopy integration scheme. *Remote sensing of environment*, *42*(3), 187-216.

Turner, D. P., Ritts, W. D., Styles, J. M., Yang, Z., Cohen, W. B., Law, B. E., & Thornton, P. E. (2006). A diagnostic carbon flux model to monitor the effects of disturbance and interannual variation in climate on regional NEP. Tellus B: Chemical and Physical Meteorology, 58(5), 476–490. https://doi.org/10.1111/j.1600-0889.2006.00221.x

Turner, D. P., Urbanski, S., Bremer, D., Wofsy, S. C., Meyers, T., Gower, S. T., & Gregory, M. (2003). A cross-biome comparison of daily light use efficiency for gross primary production. Global Change Biology, 9(3), 383–395. https://doi.org/10.1046/j.1365-2486.2003.00573.x

Chapter 4:

RESULTS

This chapter will be grouped and presented by specific research objectives provided in the introduction. Sections 4.1 to 4.8 correspond to results for objectives 1 – 3, and the rest corresponds to results for objectives 4 – 6. Results from environmental data for 2018 and 2020 are discussed separately based on their usage in different objectives.

4.1. Environmental and Tide Level Data

Daily time courses of tidal inundation over the soil surface are shown in Fig. 4a for July 11-27, 2020. A horizontal dashed line indicates tide heights that inundated the BOC MONI – HEAD at 35 cm above the soil surface. Two tide peaks were recorded on most days, and tidal flooding rarely exceeded 25 cm above the soil surface during the beginning of sampling (July 11-15). However, in the latter half of July, the maximum tide height was > 45 cm above the soil surface, which covered the base of the stem and submerged the BOC MONI – HEAD. We, therefore, designated three conditions of tidal inundation from the whole plant perspective, including fully submerged, partially submerged, and air-exposed. In our study, air-exposed indicates leaves that are exposed to the atmosphere. Partially submerged represents conditions when leaves at the height of BOC sensor are exposed to the atmosphere, but leaves below the BOC sensor are fully submerged. This is a transient period for plants between getting submerged in the rising tide (tide moves in) and being exposed with the receding tide (tide moves out). Fully submerged indicate conditions when the BOC leaves are completely submerged by the tide

while the TOC leaves are still air-exposed. TOC leaves were never fully submerged during our sampling period. We also selected mid-day flooding that peaked between 10:00 and 16:00 US EST to study the effect of tidal inundation on the photosynthetic performance of *S. alterniflora*, following Kathilankal et al. (2008).

Diurnal dynamics of PAR on TOC and BOC leaves of *S. alterniflora* are shown in Fig. 4b for July 11-27, 2020. In general, the diurnal variation in PPFD shows a similar pattern on the TOC and BOC leaves, albeit leaves at BOC receive much fewer photons during midday. For example, during tide inundation on July 12, air-exposed leaves at TOC received an average 1449 ± 52.2 (mean ± SD) PPFD compared to 736 ± 35.3 (mean ± SD) mol photons m−2 s−1 received by completely submerged leaves at BOC. Results will be presented in the form of mean ± standard deviation (SD) in the rest of the paper unless otherwise noted.

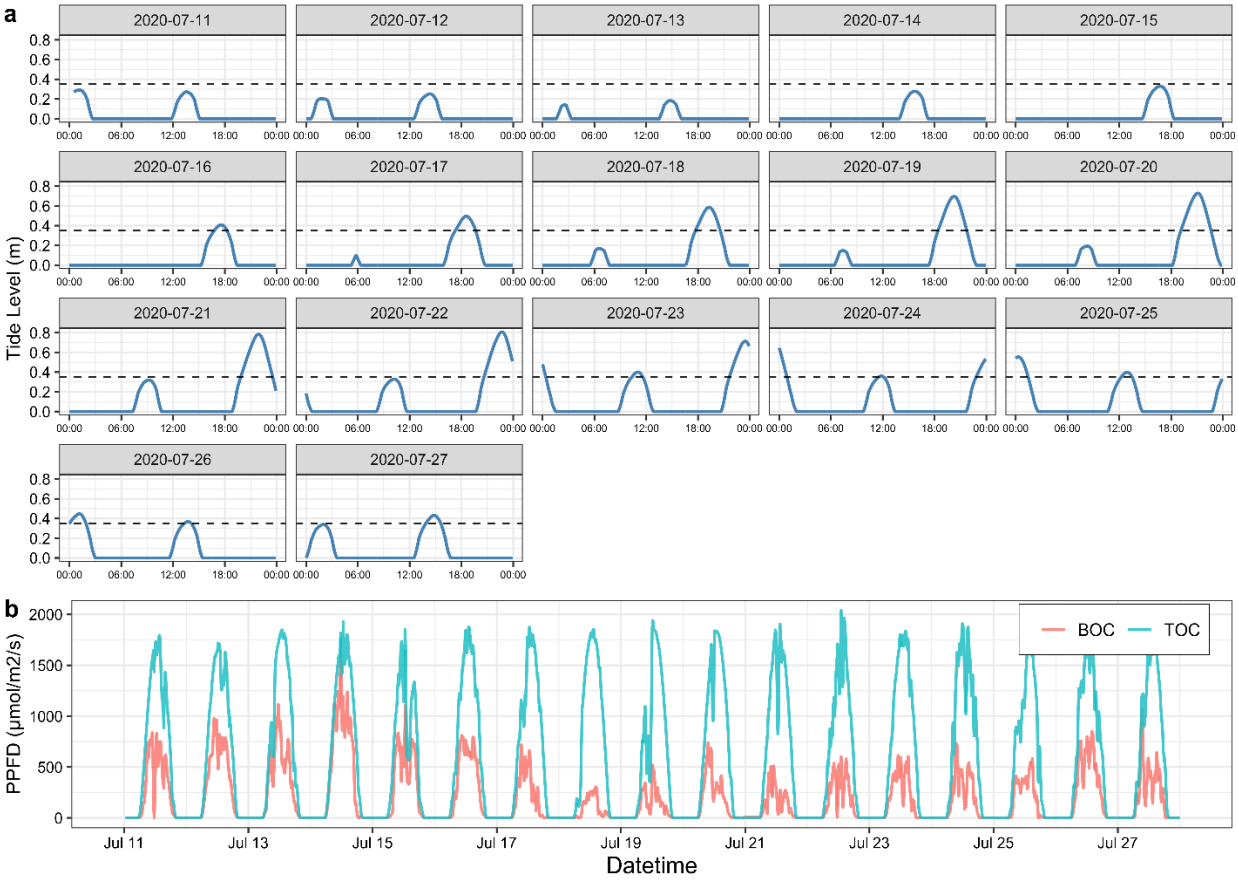

Figure 4.1 Daily environmental variables collected between 11 and 27 July 2020 from *S. alterniflora* marsh at Sapelo Island, GA: (a) The blue line represents the daily tide cycle and highlights the tide level of each peak tide over the soil surface (= 0 cm). The dashed horizontal line indicates the deployment position of emitter-detector sensor (MONI – HEAD) at the bottom of the canopy (BOC), which becomes completely submerged when the tide height is > 35 cm from the soil surface. Note that the top of canopy MONI – HEAD at 105 cm, were never submerged during the study. (b) The green and red lines illustrate the diurnal change pattern and peak of photosynthetic photon flux density (PPFD) incident on TOC and BOC leaves of *S. alterniflora*, respectively. BOC Leaves received diminished PPFD compared to leaves at TOC.

4.2. Diurnal Leaf-Level Fluorescence Variations

An example of the continuous TOC and BOC ChlF parameters measured by PAM fluorometers is shown in Figure 4.1 for July 27, 2020. July 27 was the 4th day in a row when the maximum tide level reached > 45 cm over the soil surface. The fluorescence yields observed from leaves in the dark showed differences in the fluorescence yield within the canopy. For example, F_0 measured from the TOC leaves were 2 times greater than BOC leaves (TOC F_0 range: 200.25 ± 4.14; BOC F_0 range: 102.47 ± 3.75). F_m measurements followed a similar ratio, with higher TOC F_m and lower BOC F_m (TOC F_m = 906 ± 2.74; BOC F_m = 469 ± 2.83). However, we found similar F_v/F_m (mean = 0.78) on both TOC and BOC leaves (Figure. 4.2).

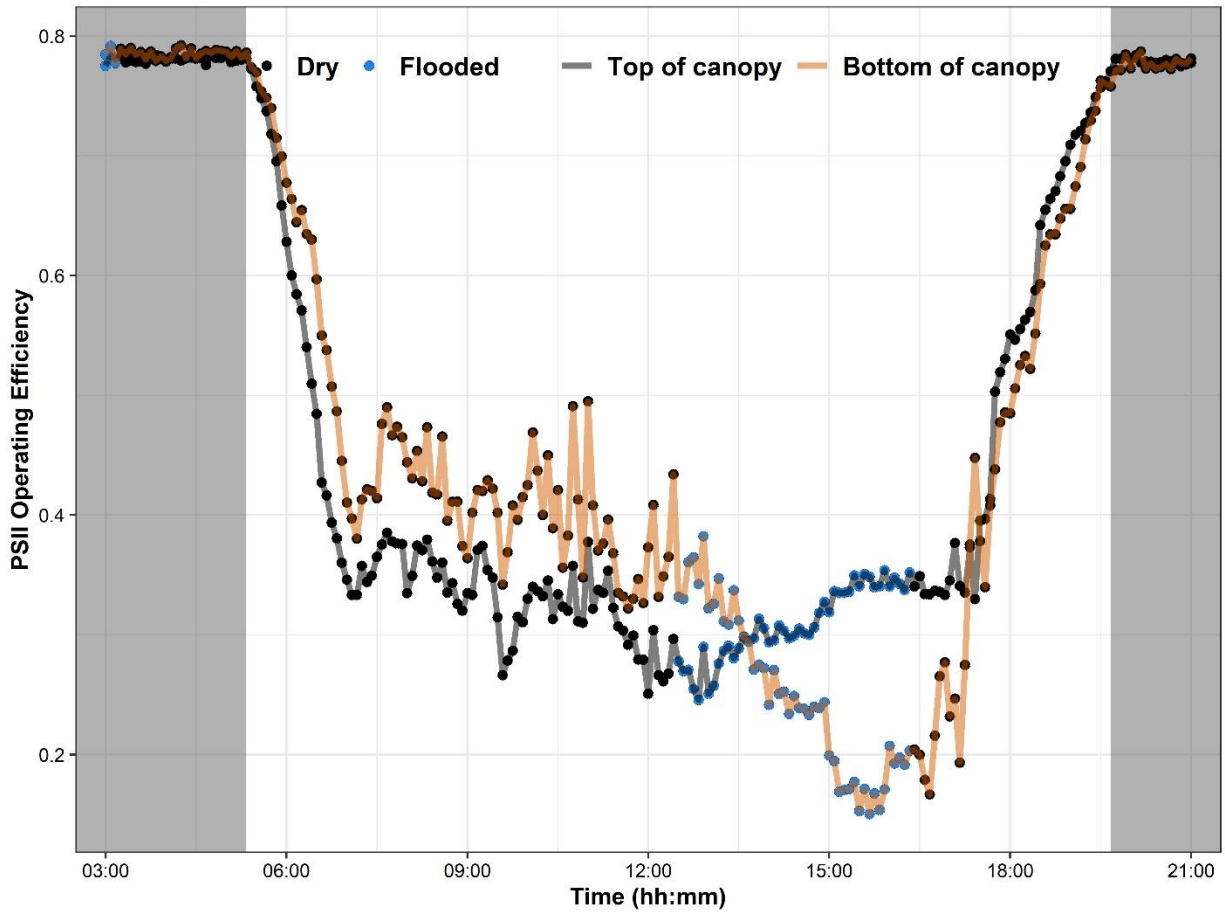
Dry
Flooded
Top of canopy
Bottom of canopy
PSII Operating Efficiency
0.8
0.6
0.4
0.2
03:00
06:00
09:00
12:00
15:00
18:00
21:00
Time (hh:mm)

(a)

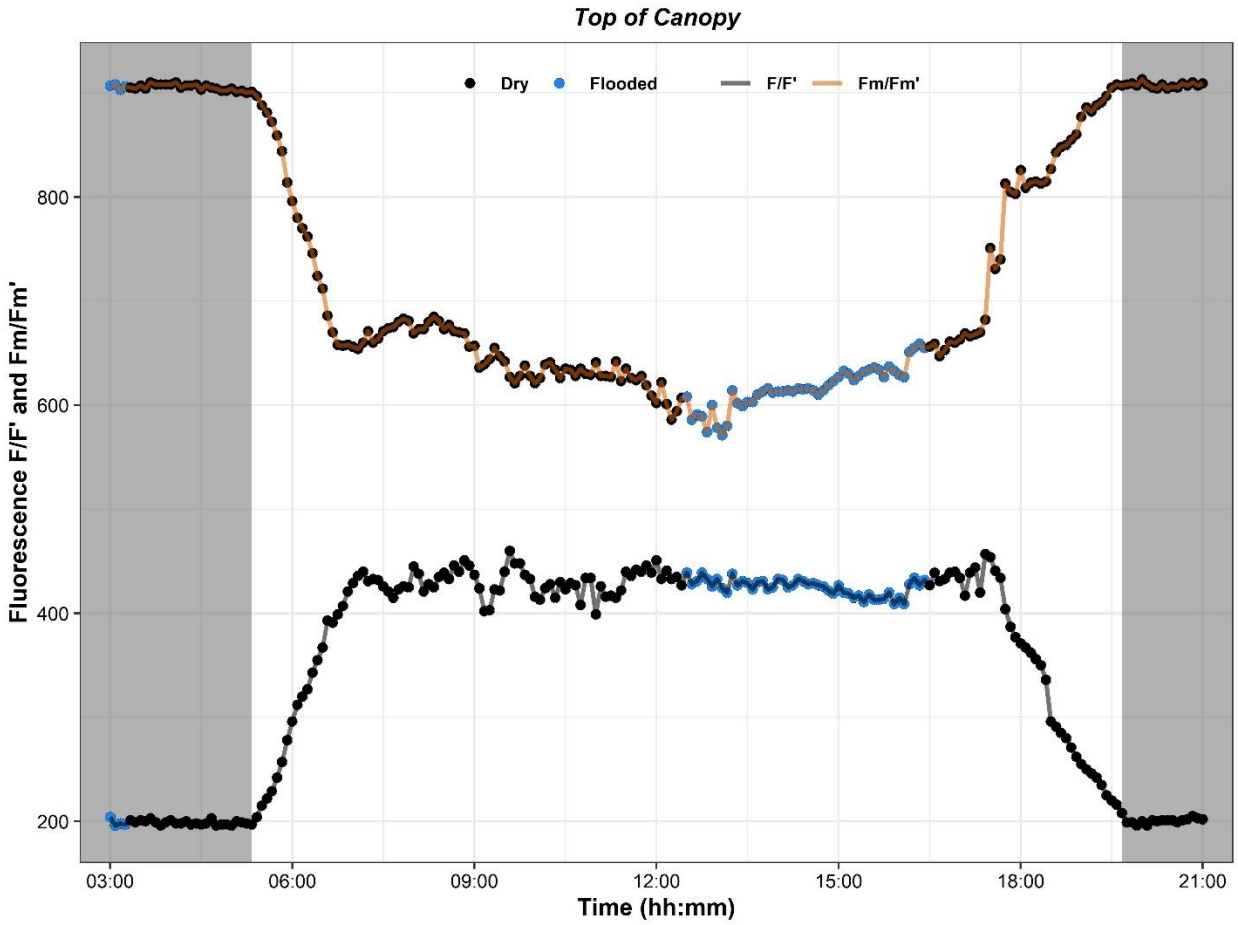
Top of Canopy
Dry
Flooded
F/F'
Fm/Fm'
Fluorescence F/F' and Fm/Fm'
800
600
400
200
03:00
06:00
09:00
12:00
15:00
18:00
21:00
Time (hh:mm)

(b)

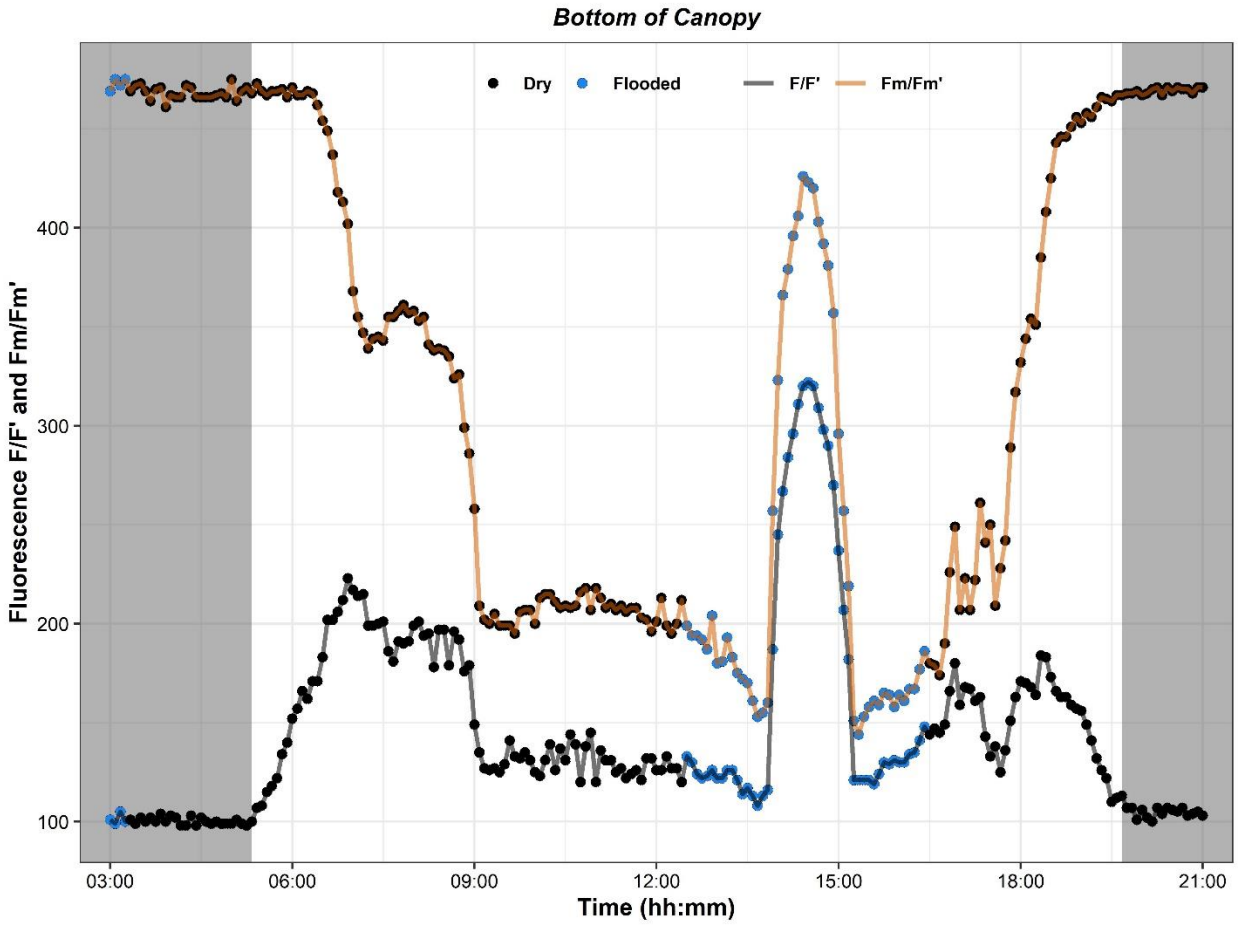

(c)

Figure 4.2 Diurnal dynamics of chlorophyll fluorescence (ChlF) parameters observed at 5-min intervals during a high tide period that occurred in the middle of the day on 27 July 2020: (a) PSII operating efficiency (φPSII) at the top of the canopy (TOC) (105cm, black line) and bottom of the canopy (BOC) (35cm, orange line); (b) & (c) maximum ChlF (orange line) and current ChlF emissions (become F_0 at night) (black line) observed from the TOC and BOC, respectively. Blue points indicate the variation in ChlF parameters during tidal flooding when the maximum tide height was 45 cm above the soil surface, which should significantly submerge the BOC sensor head. The shaded area indicates nighttime observations when Photosynthetic photon flux

density (PPFD) = 0, a prime (') notation used after ChlF parameters that represent daytime measurements when photosynthesis is occurring.

4.3. Diurnal Leaf-Level Fluorescence Variations at the top of the Canopy

Diurnal variations of F′ and F_m' illustrate responses of PSII to within canopy differences in the natural environment (i.e., natural light and heat stress) (Table 4.1). The TOC F′ and F_m' variations can be grouped into three general stages (Figure 4.2 b). *First*, after sunrise (TOC PAR > 0), F_m' started decreasing immediately, and F′ rose sharply with a corresponding reduction in F_m'. These phenomena denote that the TOC leaves are highly sensitive to PPFD and heat increases after sunrise, indicated by a decrease in F_m'. However, a decrease in the ability to oxidize Q_A, indicated by a more dramatic increase in F′ (Table 4.1), is the main factor that determines the change of φPSII after sunrise (Baker, 2008; Maguire *et al*., 2020). *Second*, both F_m' and F′ changed in a similar fashion during the day despite tidal inundation at the BOC. For example, F′ and F_m' stayed relatively constant with an average midday range of 459 ± 11 and 614 ± 17, respectively. The lowest F_m' occurred in the early afternoon (F_m' = 571 at 13:05), when the ambient air temperature was 31.59 ℃, and light radiation was intense at 1953 $\mu mol \cdot m^{-2} \cdot s^{-1}$. This daytime change pattern of fluorescence yields in *S. alterniflora* during flooding is similar to those that were reported in *Pinus sylvestris, Fagus sylvatica,* and *Cucurbita pepo* (Bilger *et al*., 1995; Porcar-Castell *et al*., 2008; Porcar-Castell, 2011). Therefore, all of these observations illustrate that fluorescence yields at the top of the marsh canopy are only slightly affected by tidal flooding as long as the top of the canopy is air-exposed, even at times when the BOC is submerged. *Third*, in the early evening, both F′ and F_m' experienced recovery with a steady decline of F′ and a constant rise in F_m'. This recovery was almost completed before darkness

when the measurements of F′ and F_m′ reached close to F_0 and F_m, respectively. No obvious fluctuations in fluorescence yields were observed at night.

Table 4.1 Summary of variation of averaged chlorophyll fluorescence (ChlF) measurements after dawn (0 < PAR < 266 μmol m^{-2} s^{-1}) during the entire sampling period.

	Parameters	Dawn (0 < PPFD < 10)	Early morning (10 < PPFD < 266)	% Change of ChlF after dawn
Top of the canopy (TOC)	F′	207 ± 31	442 ± 68	+ 113%
	F_m′	877 ± 54	678 ± 98	- 22%
Bottom of the canopy (BOC)	F′	109 ± 32	182 ± 56	+ 67%
	F_m′	458 ± 22	334 ± 87	- 27%

Note: F′ measured at the top of *S. alterniflora* canopy increased by 113% on average after sunrise, while simultaneously, F_m′ decreased on average by 22%. Overall, F′ and F_m′ measurements from the BOC present similar patterns of variation with the TOC observations after dawn but with differences in the magnitude of fluctuation. *Note:* The unit of PAR is μmol·m^{-2}·s^{-1}

4.4. Diurnal Leaf-Level Fluorescence Variations at the Bottom of the Canopy

Diurnal variation of fluorescence yields at the BOC also had three general stages, but it was more complex and variable due to the influence of tidal inundation, which sometimes submerged the BOC leaves (Figure 4.2c). *First*, after sunrise, F′ increased immediately, but F_m′ stayed constant and started decreasing about 1 hour later. *Second*, fluorescence yields at the

BOC present similar patterns of variation with the daytime TOC observations but with differences in the magnitude of fluctuation. For example, F′ and F_m′ stayed steady within the range of 127 ± 4.5 and 207 ± 10, respectively, before tidal flooding (Figure 4.2c). However, tidal inundation led to large fluctuations in fluorescence yields in the BOC leaves. For example, on July 27, 2020, the tide started rising at 12:35, peaked at 14:35, at a height that submerged the BOC leaves, and then gradually decreased until it completely subsided at about 16:25. When tides were highest, a maximal F_m′ of 426, which is close to Fm, was observed. F′ also rose sharply to a maximum that was above even the highest F′ from the morning observation period. Water from tidal flooding is a good absorber of both light and heat energy. Thus, the cool, low light environment provided during BOC flooding likely corresponds to minimal levels of NPQ, with the concomitant closure of the majority of PSII reaction centers that would likewise prohibit photochemistry. Thus, most of the light energy absorbed by PSII was lost as ChlF during this time. *Third*, in the early evening, F′ and F_m′ started returning to levels close to those before sunrise. Although in-situ ChlF measurements have been reported for salt marshes (Kathilankal *et al*., 2008), our time series of daily ChlF dynamics, for the first time, provides continuous leaf-level information on the acclimation of PSII to realistic field tide inundation in *S. alterniflora* at different canopy heights.

4.5. Diurnal Leaf-Level Variations of Quantum Efficiency of PSII

Figure 4.2a depicts the variation of F_v/F_m and φPSII calculated from the TOC and BOC ChlF. In general, during the high tide day, BOC φPSII was higher than TOC φPSII. For example, the mean BOC φPSII, excluding midday tidal inundation, was 0.39 ± 0.05 compared to the TOC φPSII of 0.298 ± 0.03 (Table 4.2). During tidal inundation, there were no detectable changes in TOC φPSII efficiency, but the BOC leaves showed a considerable reduction in φPSII,

as φPSII closely followed the height of tidal flooding with minimal values below 0.2 during the BOC submergence. Our results suggest that the PSII reaction centers in fully submerged *S. alterniflora* leaves were still active and transferring electrons, but only at approximately 20% of the typical daily rate. This is a new finding, and to our knowledge, these differences in leaf-level reductions in φPSII within *S. alterniflora* canopy at different stem heights under natural flooding conditions have not been reported before in the literature.

Averaged F_v/F_m for the *S. alterniflora* leaves from TOC and BOC showed a similar value of F_v/F_m at 0.78 (TOC: 0.78 ± 0.002; BOC: 0.78 ± 0.004), which is slightly lower than the optimal value reported for many plant species (Björkman & Demmig, 1987; Bilger *et al*., 1995; Murchie & Lawson, 2013; Yang *et al*., 2017). To our knowledge, this F_v/F_m has not been reported before for *S. alterniflora* in real-field conditions either. F_v/F_m is thought to reflect the maximum quantum efficiency because leaf-level fluorescence parameters were continuously measured through the night when Q_A was supposed to be maximally oxidized, and the level of heat loss from PSII (NPQ) should have disappeared completely (Maxwell & Johnson, 2000). However, we found that NPQ stayed more or less active at night during our sampling period (averaged nighttime NPQ = 0.086 ± 0.013), which lowered F_m and resulted in a smaller F_v/F_m. This phenomenon has been reported before and described as a common occurrence during summer months with higher night temperatures (Porcar-Castell *et al*., 2008; Yang *et al*., 2017). Those conditions represent our site well, where summer nights in coastal Georgia, USA are typically warm and humid. In addition, photoinhibition caused by frequent saturating pulses from PAM fluorometer may have led to a decrease in F_m, resulting in a smaller F_v/F_m at night (Porcar-Castell *et al*., 2008).

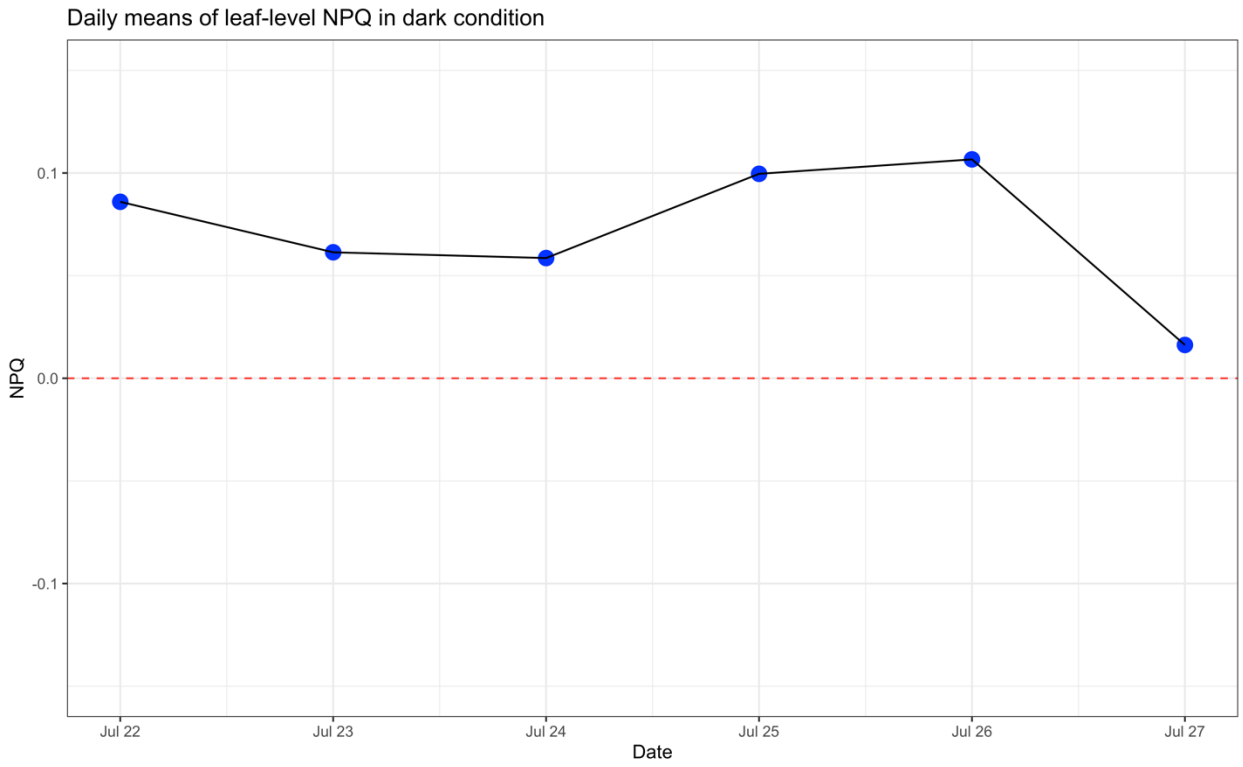

Figure 4.3 Daily means of NPQ in dark conditions. This suggests NPQ of *S. alterniflora* stayed active at night during our sampling period

4.6. Response of PSII Working Efficiency(φPSII) to Tide Heights during Low Tide Flooding

The effect of tidal flooding on φPSII was observed during the daytime. The measured φPSII were plotted against tide height when flooding occurred between 10:00 AM and 16:00 PM and tide heights did not reach the BOC sensor (Figure 4.4). During these low tide days (peak tide height at ~25 cm), our data did not show substantial fluctuations of TOC and BOC φPSII.

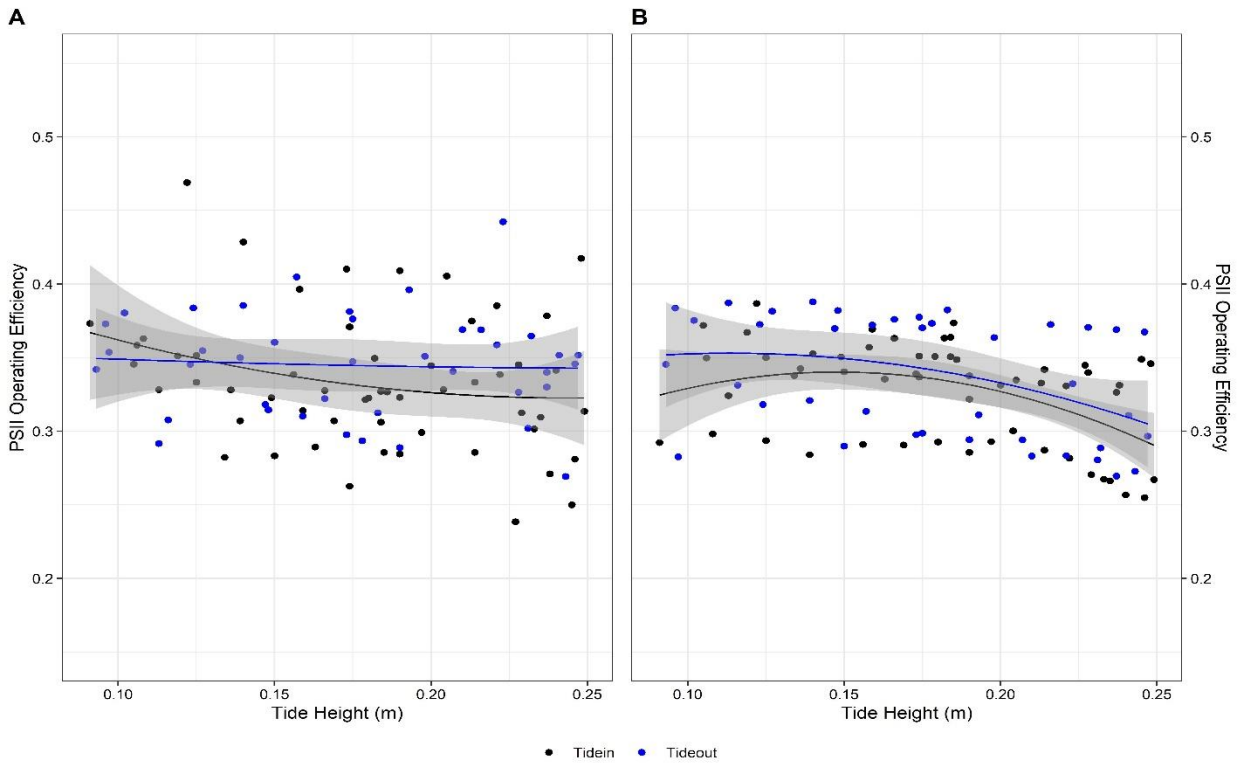

Figure 4.4 The responses of photosystem II operating efficiency (φPSII) at the (A) bottom (BOC, 35 cm) and (B) top (TOC, 105 cm) of the *S. alterniflora* canopy to increasing water table height during low tide days with 25 cm peak tide level above the soil surface.

4.7. Response of PSII Working Efficiency(φPSII) to Tide Heights during High Tide Flooding

The measured φPSII were also plotted against tide height tide on higher tide days when the BOC sensor was completely submerged during tidal inundation (Figure 4.5). The BOC φPSII showed sizeable reductions as they were negatively associated with tide height (Figure 4.5a). For example, BOC leaves φPSII dropped from an average of 0.39 ± 0.05 in air-exposed conditions from the start of the tide (non-flooded) to 0.33 ± 0.06, in partially submerged conditions as the tide level gradually rose (tide height < 0.35 cm). The relationship became more pronounced when the tide height > 35 cm completely covered BOC *S. alterniflora* leaves. This resulted in a

greatly reduced φPSII rate in fully submerged leaves. For example, the rate of BOC φPSII for fully submerged leaves declined on average by 41% compared to air-exposed leaves in non-flooded conditions (Table 4.2). In contrast, the impact of high flooding on φPSII in air-exposed TOC leaves was low, with less than 10% decline on average, at times when the BOC leaves were completely submerged.

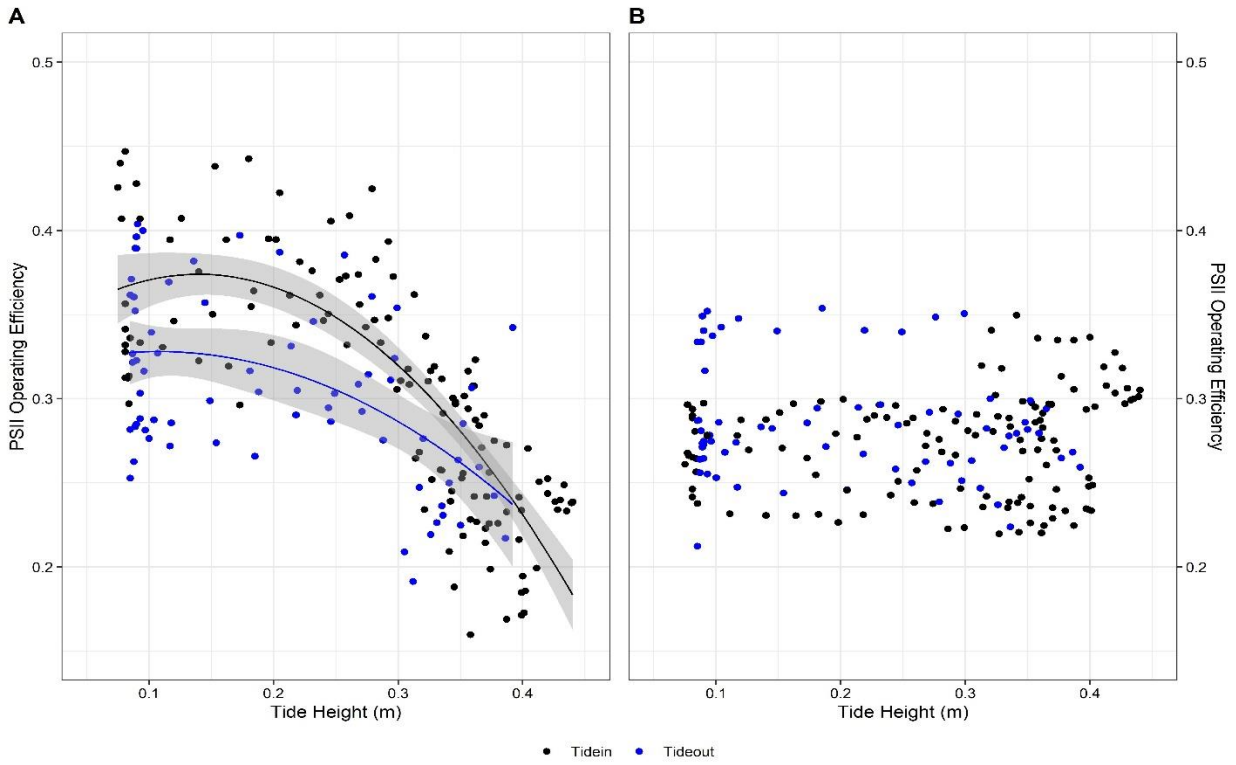

Figure 4.5 The responses of photosystem II operating efficiency (φPSII) at the (A) bottom (BOC, 35 cm) and (B) top (TOC, 105 cm) of the *S. alterniflora* canopy to increasing water table height during high tide days with > 45 cm peak tide level above the soil surface.

4.8. Overall Response of PSII Working Efficiency(φPSII) to Tide Heights

In summary, the results (Table 4.2) demonstrate the applicability of PAM fluorometry to continuously track photochemical and non-photochemical PSII quantum yields in salt marshes in the field under a range of tidal and light conditions. Our field observations on the relationship

between leaf-level *S. alterniflora* ChlF and tide levels showed that photochemical efficiency differed markedly based on leaf submergence. The rate of φPSII in fully submerged BOC leaves decreased significantly compared to air-exposed leaves due to the physiological stresses induced by tidal inundation. For example, the lower diffusion rate of gases and increased rate of stomatal closure act as major restrictions for fully submerged leaves (Heinsch et al., 2004; Knox et al., 2018), suggesting that underwater φPSII is PQ instead of NPQ-limited. Additionally, we observed greatly reduced underwater photosynthesis activities in fully submerged leaves, suggesting that *S. alterniflora* could potentially remain a CO2 sink during tidal inundation (Artigas et al., 2015, Huang et al., 2020).

Table 4.2 Variation of PSII operating efficiency (φPSII) at the top (TOC) and bottom (BOC) of the S. alterniflora canopy during (a) high tide and (b) low tide flooding.

a	High Tide Flooding					
	TOC			BOC		
Tide height	0 – 35cm	>= 35cm	Dry*	0 – 35cm	>= 35m	Dry*
Sensor submergence	Air-exposed	Air-exposed	Air-exposed, no canopy flooding present	Air-exposed	Fully submerged	Air-exposed, no canopy flooding present
φPSII (Mean ± Sd)	0.28 ± 0.03	0.28 ± 0.03	0.3 ± 0.03	0.33 ± 0.06	0.23 ± 0.05	0.39 ± 0.05

% Changes	- 7.0%*		- 7.0% *		-15.4%*	- 30.3 %	- 41% *	

b	Low Tide Flooding			
	TOC		BOC	
Tide height	0 – 25cm	Dry*	0 – 25cm	Dry*
Sensor submergence	Air-exposed	Air-exposed, no canopy flooding present	Air-exposed	Air-exposed, no canopy flooding present
φPSII (Mean ± Sd)	0.33 ± 0.03	0.36± 0.04	0.34± 0.04	0.40 ± 0.05
% Changes	-8.3%*		-15%*	

Note: The table show Changes (%) in φPSII for *S. alterniflora* leaves between air-exposed, partially submerged, and fully dry (non-flooded) conditions during high tide when the maximum tide height fully submerged BOC MONI – HEAD and during low tide when both TOC and BOC MONI – HEAD are air-exposed during the maximum tide. Asterisks (*) denote percent changes in φPSII at different tide heights. There were pronounced reductions in φPSII in partially or fully submerged *S. alterniflora* leaves compared to non-flooded conditions. We observed less than 10% changes in φPSII in air-exposed TOC during both tidal events.

4.9. Environmental Data for the Random Forest Model

Our random forest model used PAR and tide level data as well as the four other predictors to model the relationship between *S. alterniflora* φPSII and environmental gradients.

Figure 4.6 presents all environmental variables, including diurnal air temperature (Tair; C°), diurnal soil temperature (Tsoil; C°), diurnal water level relative to the marsh soil surface (WT; m), diurnal incident PAR (PAR; μmol photons/m^2/s) and diurnal cloudiness index (CI) that continuously collected for two experimental sites during the two sampling years. Figure 4.6 does not include interpolated NIRv as the plant phenology didn't change significantly during our relatively short sampling period (see section 3.9). In addition, we used the same method explained in Chapter 3 to post-process the entire dataset.

These two sites experienced similar climates although differing in sampling period (Figure. 4.5). For example, during the sampling, Tair had similar ranges, but July 2020 tended to peak at a higher Tair at midday. This followed the seasonal pattern that we expected, with fall (later August and early September) Tair being cooler than summer (July), when Tair variability was also greater. PAR was also similar at both sites. Mean midday (11:00 - 13:00) PAR was 1865 μmol/m^2/s in 2020 compared to 1789 μmol/m^2/s in 2018. However, 2018 experienced more cloudy days than 2020 during our sampling. This is shown by the higher midday CI in Figure 4.6a as well. During our sampling at the Keenan Field marsh platform in 2020, there were taller plants with dense canopy compared to the flux tower site in 2018, creating opportunities to test for differences in microclimate in each marsh zones. For example, although Tair for both sites were similar throughout the study (Fig. 1a & f), the 2018 sampling period had cooler Tsoil than the 2020 sampling period, suggesting greater soil shading. Differences in marsh canopy structure also caused greater Tsoil variability and higher peak values (Fig. 4.6b). In addition, although the elevation of both sites were similar, our two sites still experienced differences in flooding frequency and WT because the Keenan Field marsh is closer to the nearest creek and thus experiences more and higher tidal flooding. For example, in 2018, tide reached the flux tower

site for the most days, but tidal flooding rarely exceeded 0.25 m above the soil surface (6 days out of 20 days sampling periods). In contrast, the tidal flooding level was typically > 0.3 m above the soil surface (15 out of 16 days) during the 2020 sampling period. Midday WT peaked at a similar level, around 0.6 m across two sites. These environmental conditions were not significantly different across time and space, but they are good enough to make our model more comprehensive and have better compatibility.

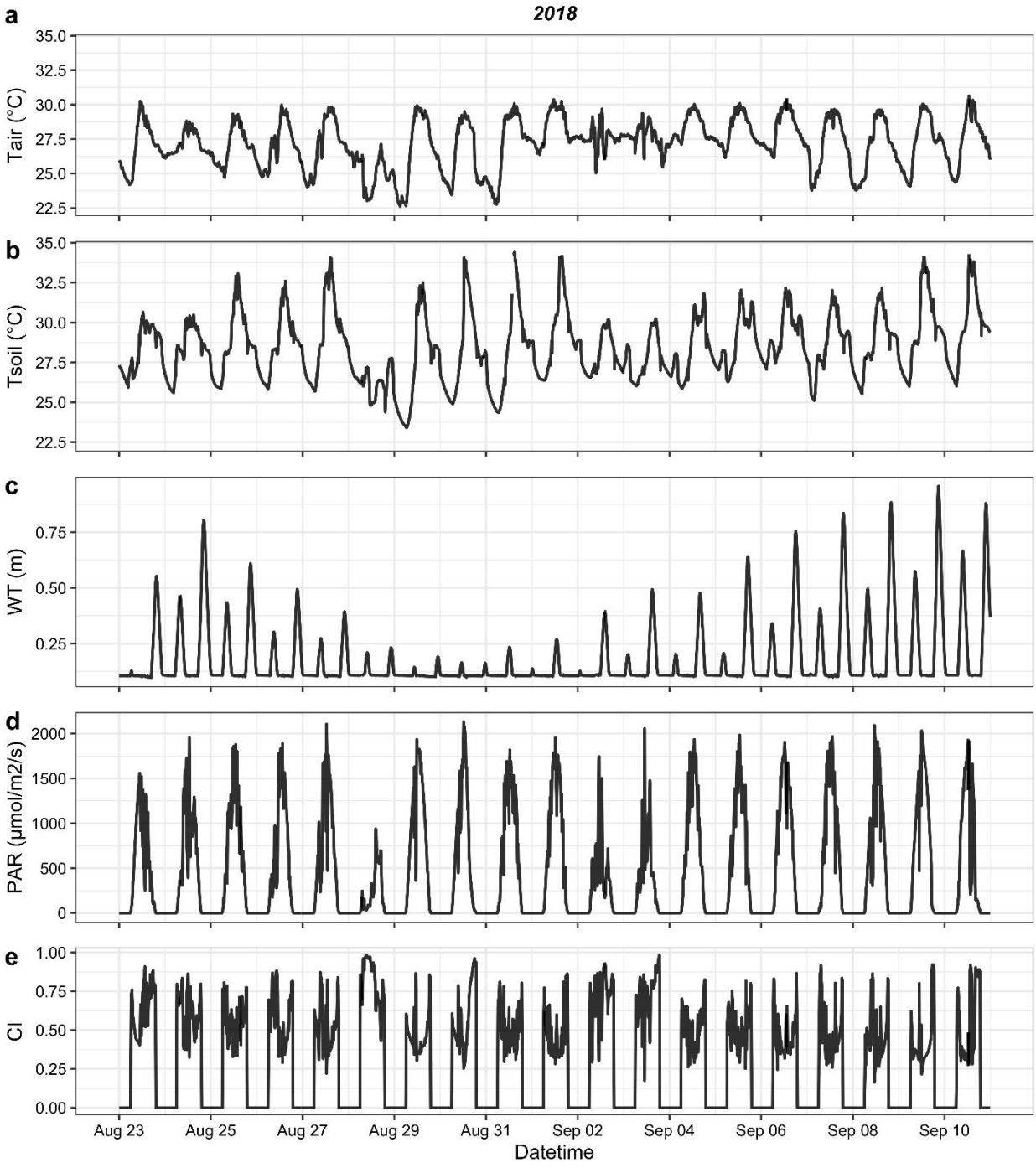
a
2018
Tair (°C)
35.0
32.5
30.0
27.5
25.0
22.5
b
Tsoil (°C)
35.0
32.5
30.0
27.5
25.0
22.5
c
WT (m)
0.75
0.50
0.25
d
PAR (µmol/m2/s)
2000
1500
1000
500
0
e
CI
1.00
0.75
0.50
0.25
0.00
Aug 23
Aug 25
Aug 27
Aug 29
Aug 31
Sep 02
Sep 04
Sep 06
Sep 08
Sep 10
Datetime

(a)

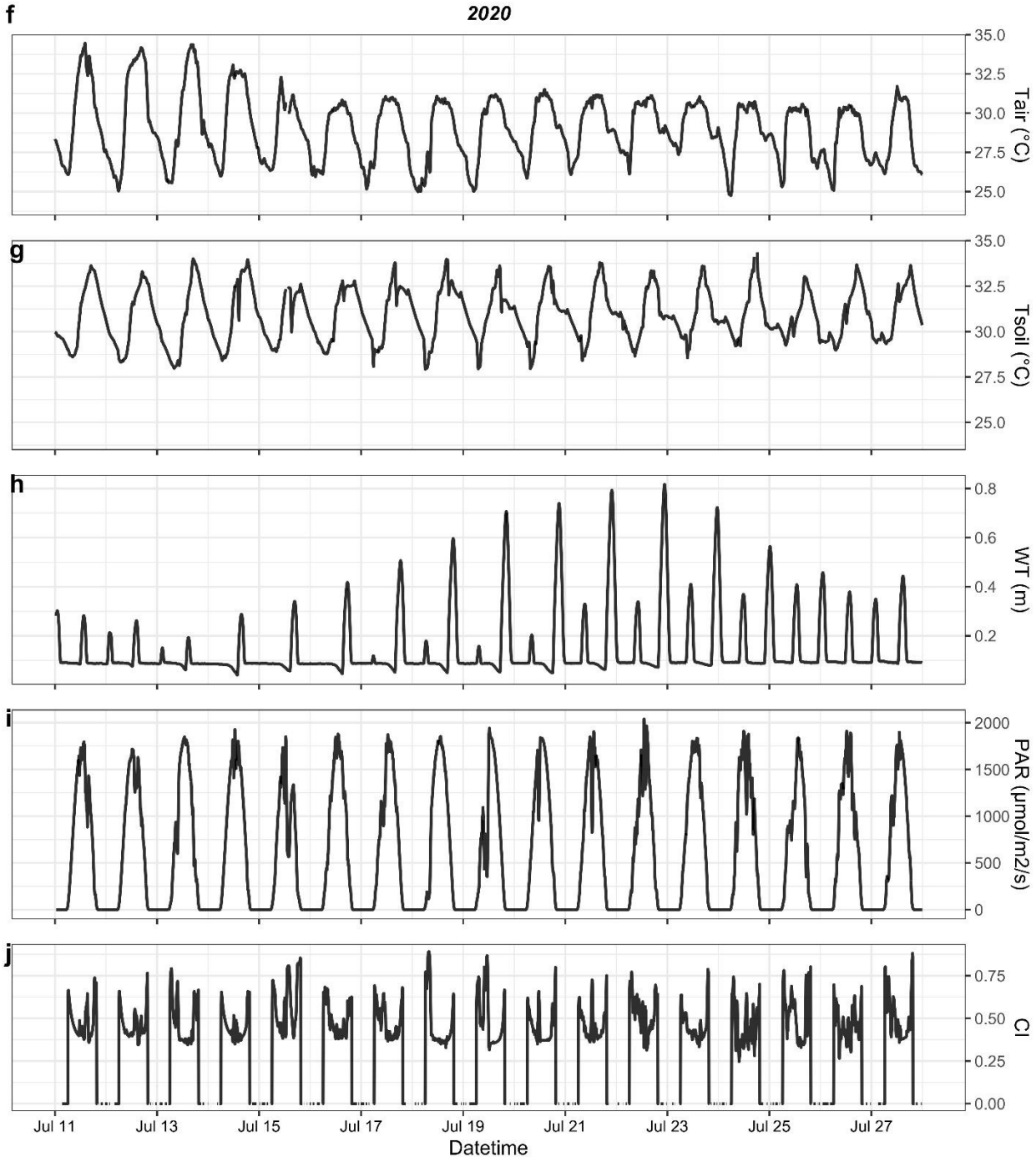

(b)

Figure 4.6 Daily environmental variables measured during (a) 2018 and (b) 2020 sampling period. 2018 data were collected from August 23 to September 10 at the flux tower site at Sapelo Island, GA. 2020 data were collected from July 11 to July 27 at Keenan field site at Sapelo

Island, GA. (a,f) air temperature (Tair), (b,g) soil temperature (Tsoil), (c,h) tide level over the soil surface (WT), (d,i) photosynthetically active radiation (PAR), (e,j) cloudiness index (CI).

4.10. Random Forest Model Tuning and Validation

We trained and validated the random forest model using hyperparameter tuning and repeated 3-Fold cross-validation to link salt marsh φPSII biophysical and meteorological variables. These measurements are commonly found and relatively reliable in the coastal ecosystem. The tuning result for the regressor parameters is shown in Table 4.3.

Table 4.3 Tuning result for the random forest regressor parameters

Cross-validation	Number of estimators	Min node size	Mtry	RMSE	R^2
True	400	5	4	0.045	0.827

The best-performing random forest models from the tuning results had 400 trees, 4 variables to randomly sample as candidates at each split, and a minimal node size of 5. The observed versus predicted φPSII of the tuned model for the training and validating datasets are shown in Figure 4.7. The RMSE between field measurements and model predictions of *S. alterniflora* φPSII for the entire training dataset was 0.045, and the RMSE increased to 0.09 after applying the final model to the global validation dataset, which was independent to the global training dataset (Figure 4.7). Both predicted and observed datasets were in the range between approximately 0.22 to 0.75, with the highest PSII prediction at around 0.71. The error was smaller than two standard deviations (2 S.D.) without a particular pattern of over or underestimation. Overall, the predicted φPSII corresponded with the field data, but we identified

a few outliers with differences greater than 0.05 at areas with low φPSII values, which indicated that there might be a slight over-prediction in the lower range (Fig. 4.7b).

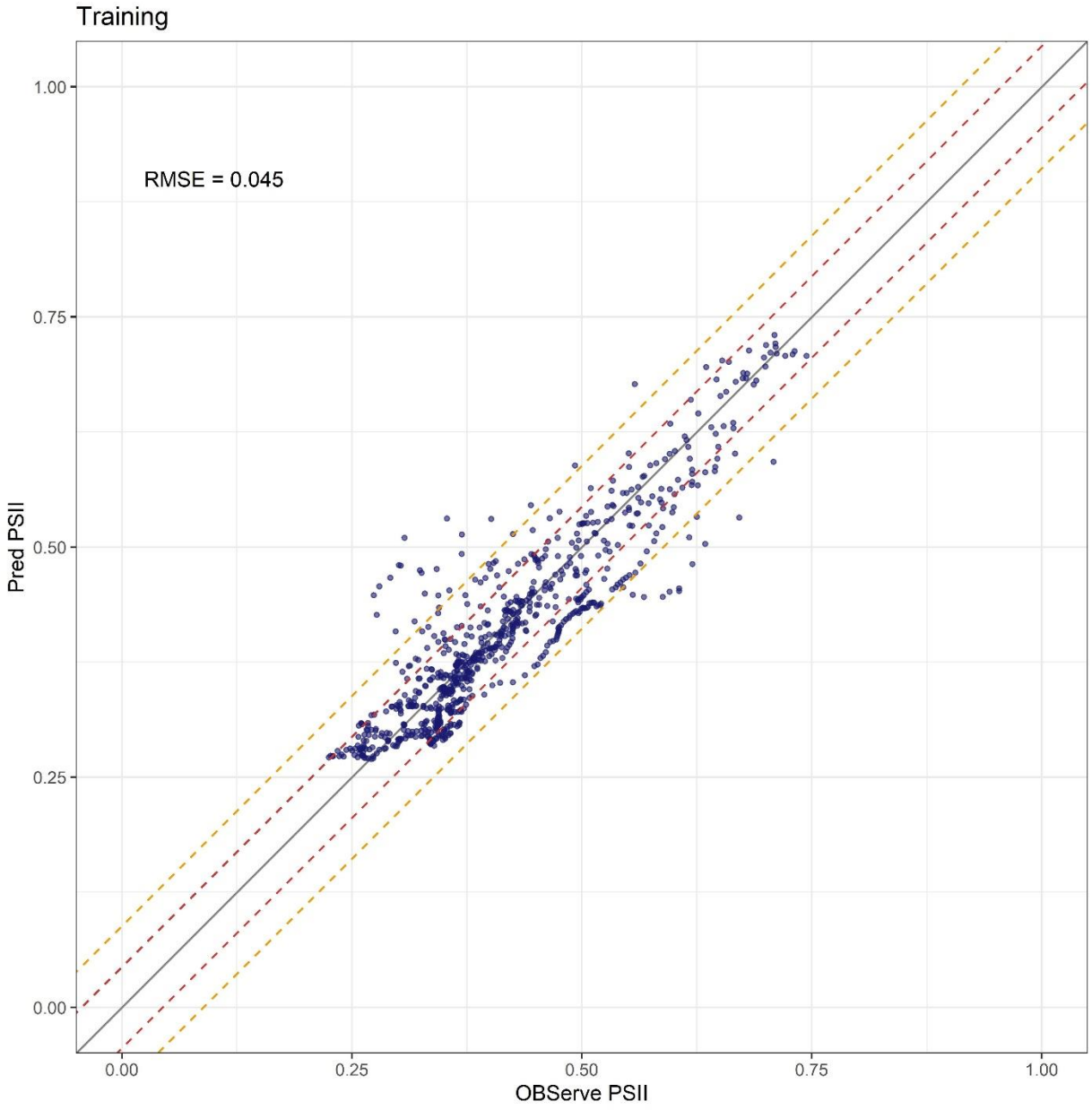

(a)

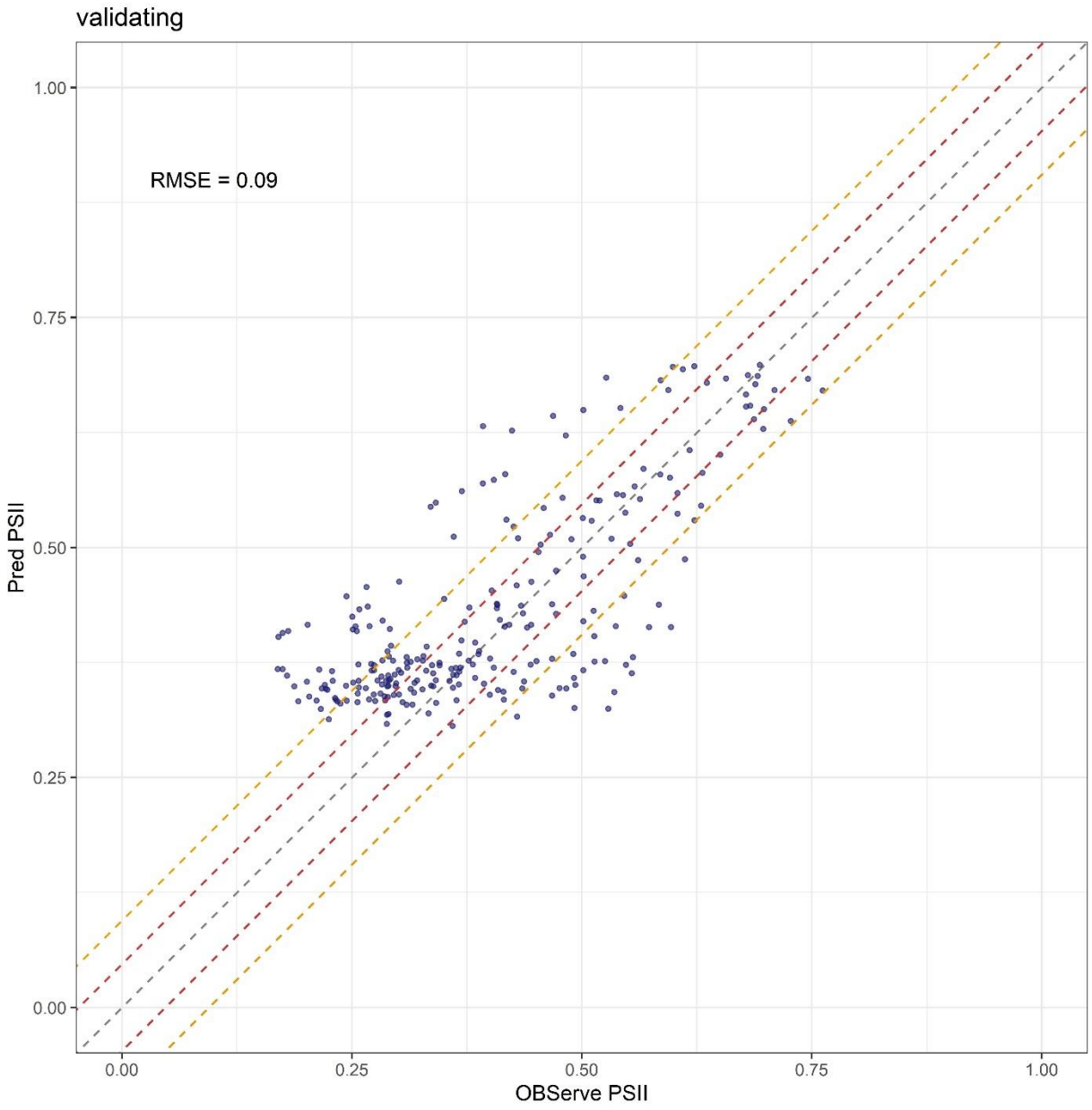

(b)

Figure 4.7 Visualization of random forest model error: Observed vs. predicted PSII and root mean squared error (RMSE) of fit between field observation and model prediction for the (a)

training datasets and (b) validation dataset with standard deviation line from the mean (dashed red: ±1 SD; dashed orange: ±2 SD)

4.11. Contribution of Variables in the Final Random Forest Model

In our model, all predictors contributed to explaining the model variance but differed in the significance level. Figure 4.8 shows the importance of the selected variable in predicting φPSII. In this instance, PAR and NIR_V have a significant impact on the model outcome because model accuracy decreases by more than 60% when PAR and NIRV are excluded. Tsoil and WT are also important to the model accuracy as removing them would cause at least 30% increases in the mean square error of the model. CI and Tair, while significant, were less important as the model accuracy only reduced by ~ 20% when they were excluded.

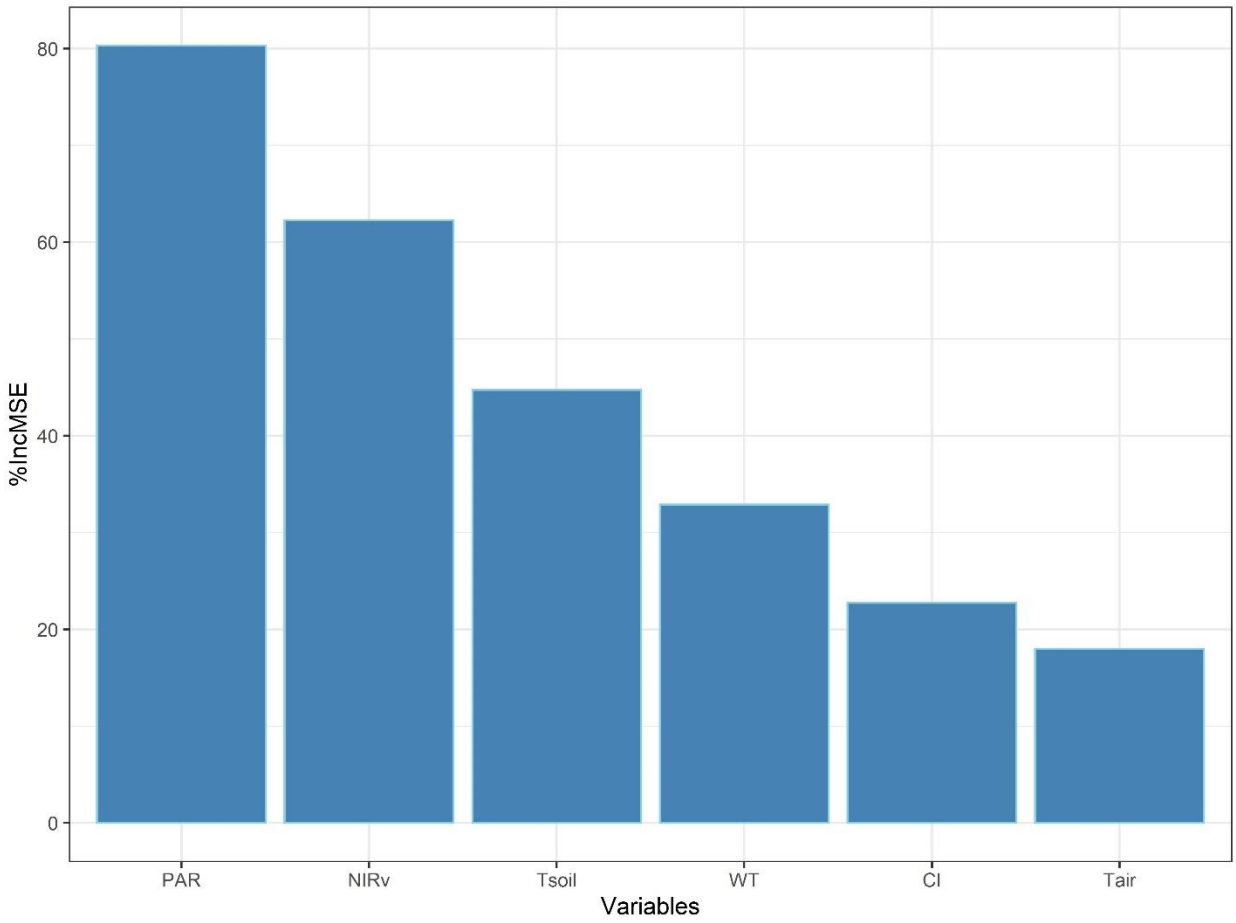

Figure 4.8 Estimated variable importance of each variable in the random forest model. Variable importance was calculated based on the percentage of accuracy decreases when the variable is excluded. Variable with high values indicating that it has more significant impacts on the model outcome.

4.12. Diurnal Variations of PSII Working Efficiency Predictions

First, we used our PSII model at the flux tower to predict PSII and analyze the diurnal model output. Predictors used in the PSII model, including Tair, Tsoil, PAR, WT, CI were available from the flux tower, NIR_V was averaged by retrieving nine pixels (3x3 grid) from Sentinel-2 images near the flux tower (Figure 4.10b). An example of predicted PSII diurnal

variation with 30-min temporal resolution of August 08, 2020, and July 31, 2020 is shown in Figure 4.9. We selected these two days in the growing season because they had similar environmental conditions, including averaged midday PAR and air/soil temperature at around 1796 μmol·m^{-2}·s^{-1} and 30.3/32.4 ℃, respectively but different tidal flooding conditions. August 08 experienced tidal flooding from 09:15 to 15:00 LST with a peak height of 0.4 m above the soil surface while on July 31, tidal flooding did not occur until later in the day (16:00 LST) (Figure. 4.9. Therefore, a comparison of predicted PSII between two days with similar environmental conditions and different tidal flooding schedules showed our model can estimate not only the diurnal variation of marsh photosynthetic activities but also the fluctuation of marsh photosynthesis under the natural coastal conditions.

From the predicted PSII graph, we can clearly see, from dawn to dusk, three general stages of marsh PSII daily variations on both days. First, predicted φPSII decreased with a corresponding increase in solar radiation after sunrise. Second, predicted φPSII stayed relatively constant during the day. For example, predicted φPSII started saturating at 10:30 LST when the solar radiation was around 1625 μmol·m^{-2}·s^{-1}, and stayed relatively unchanged throughout the noon with averaged midday PSII at around 0.31 ± 0.04. Although, at the same time, the solar radiation continued to increase and peaked at around 2000 μmol·m^{-2}·s^{-1}. Thirdly, predicted PSII started to gradually recover from early evening and continued to increase until sunset with continuously decreasing solar radiation. It eventually returned to almost the same level that it was before the sunrise.

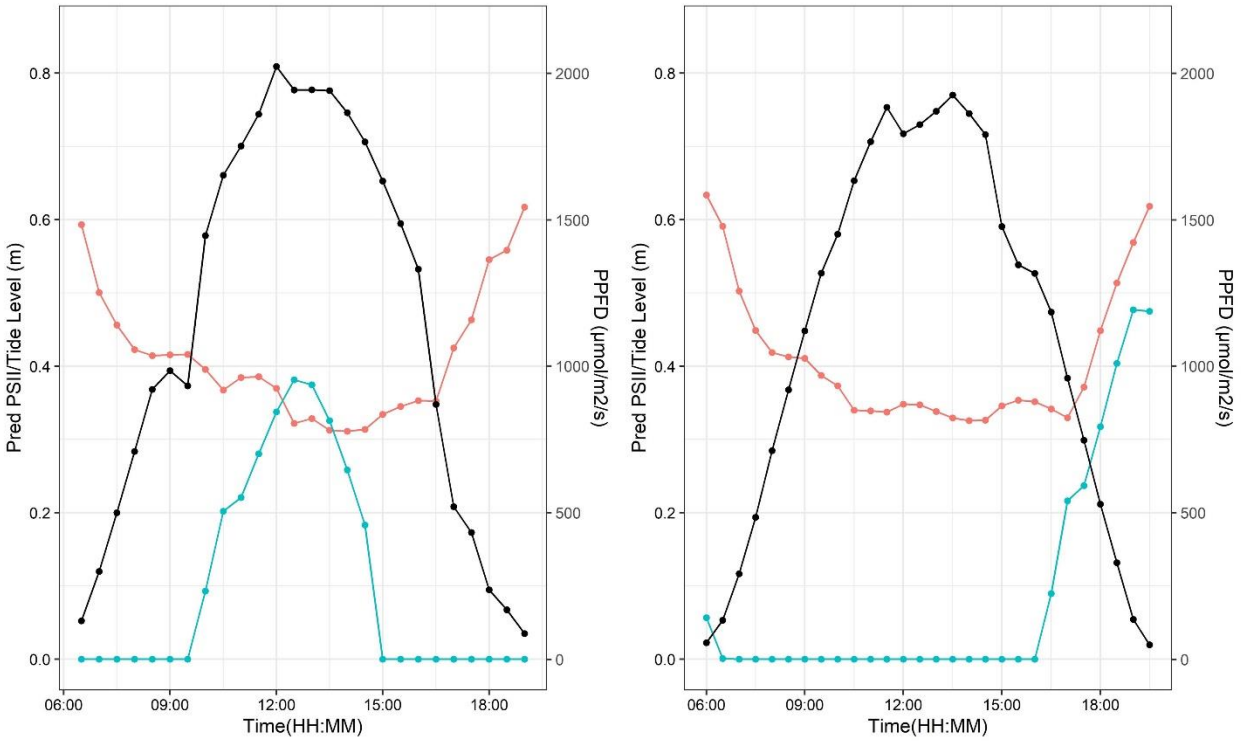

Figure 4.9 An example of our random forest model predicted diurnal dynamics of PSII operating efficiency (φPSII) (red line) at 30-min intervals on two select days with similar meteorological conditions. The blue and black lines illustrate the diurnal change pattern and peak of tide level above the soil surface and photosynthetic photon flux density, respectively. (a): predicted φPSII of 08 August 2020 with tidal flooding in the middle of the day; (b): predicted φPSII of 31 July 2020 with tidal flooding in the early evening.

4.13. The Relationship between Marsh Photosynthetic Activity and Environmental Stress

Our model effectively captured the impact of environmental stressors on marsh photosynthetic activity under natural field conditions. There were obvious fluctuations in predicted φPSII at noon on August 08, 2020 because of a midday tidal flooding where the maximum tide level reached > 35 cm over the soil surface. Specifically, the model predicted φPSII did not continue declining or showed signs of saturation with increasing solar radiation

between 10:30 - 11:30 LST. Instead, it increased along with the incoming tide and then began falling as the tide continued to rise, peaking at 12:30 LST (Figure. 4.9a). This suggests that our φPSII prediction is highly sensitive to environmental changes in the marsh ecosystem even when it is saturated under high solar radiation, which is critical for studying changes in salt marsh photosynthesis. However, tidal flooding in the early evening showed little effect on the marsh photosynthetic activities (Figure 4.9b). For example, there were some decreases in predicted φPSII starting at 16:00, but tidal flooding did not affect the overall recovery pattern of φPSII in the late evening with a corresponding reduction in PAR, as shown on July 31. This indicated the dominance of PAR in plant photosynthesis under unsaturated conditions and explained why it is the most important predictor in our random forest model. However, the important contributions of other predictors to model predictions cannot be ignored (Figure 4.8). For example, in the morning and late afternoon, our predicted φPSII is highly fluctuated which reflects the importance of NIR_V because plant exposed to actinic light from nighttime and when the continuous actinic light gradually fades away would affect the redox state of primary quinone electron acceptor of PSII (Q_A) and leading to changes in fPAR. During the rest of the day, especially at midday when PSII is saturated with high levels of solar radiation, tidal flooding and the corresponding environmental changes (such as lower soil temperature) may alter our φPSII predictions. This highlights the importance of the bottom-up model for studying the photosynthesis of salt marshes in coastal wetlands because the generalizations of top-down models may omit the rapid responses of salt marshes to environmental changes (i.e., a rapid adjustment in the energy partition inside chloroplast), which can lead to over or underestimation of salt marsh productivities at the ecosystem level.

4.14. Monthly Variations of Predicted PSII Working Efficiency

We applied our model to predicted time series for *S. alterniflora* φPSII for a broader spatial and temporal scale. Figure 4.10 presents an example of the estimated 3-m resolution PSII for the 2020 growing season between April and October across three different height forms of *S. alterniflora* within the GCE flux tower footprint. This provided rich spatiotemporal information on φPSII for *S. alterniflora* marshes around the Sapelo Island flux tower. For example, predicted φPSII was the highest adjacent to creeks and marsh exterior, which is dominated by tall *S. alterniflora* and was the lowest in the southwest of the assessment area in late spring (May). This spatial distribution pattern changed in the summer months (July and August) when predicted φPSII was highest in the marsh interior and lowest adjacent to creeks. This could be attributed to higher inundation effects (e.g., inundation frequency and water depth) on the photosynthesis of medium *S. alterniflora* in areas with dense creek networks (Figure 4.10b)

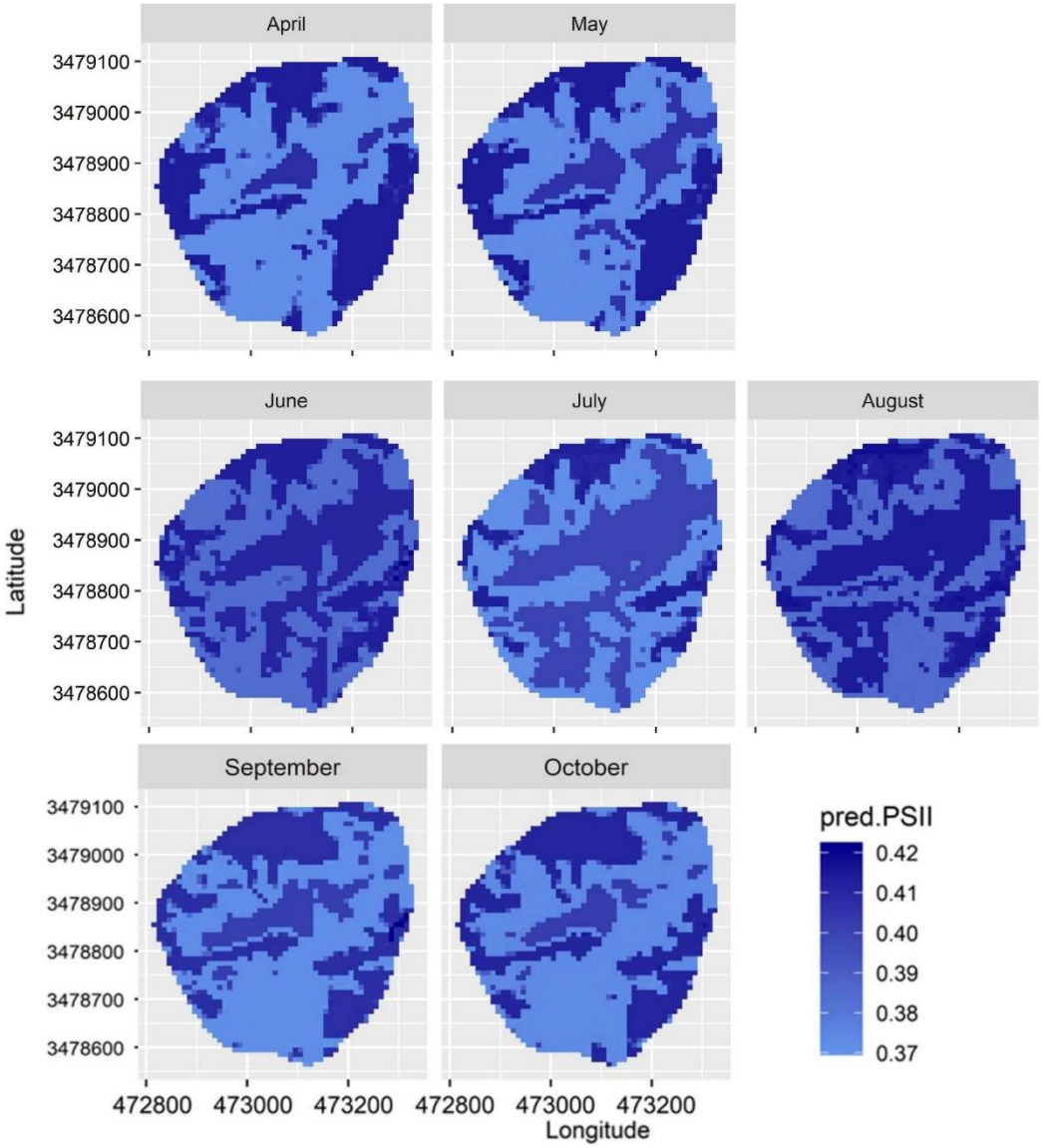
April
May
June
July
August
September
October
Latitude
3479100
3479000
3478900
3478800
3478700
3478600
472800
473000
473200
Longitude
pred.PSII
0.42
0.41
0.40
0.39
0.38
0.37

(a)

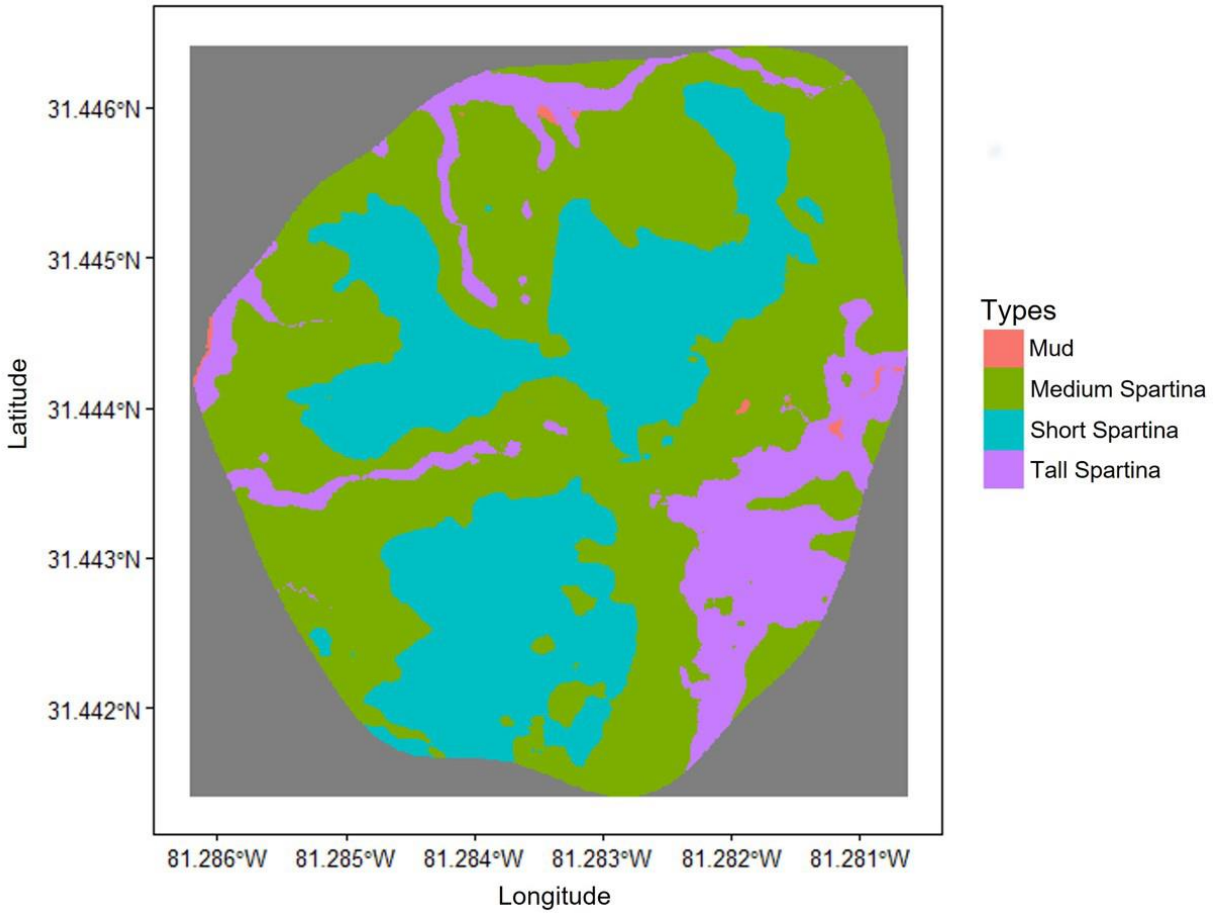

(b)

Figure 4.10 (a) A seasonal comparison of random forest model predicted φPSII from April to October for the entire flux footprint, lighter blue indicates areas with higher PSII predictions. (b): A 1-m spatial resolution habitat map of the flux footprint showing the distribution of different *S. alterniflora* forms.

This predicted PSII also showed differences in seasonal variation across the *S. alterniflora* forms. For example, areas of short to medium *S. alterniflora* in the marsh interior (Figure 4.10b, blue) showed double peaks, one early in the growing season (June) and the other in August. Correspondingly, the minimums appear in late fall (October) and early spring months (April). Tall *S. alterniflora* (Figure 4.10b, purple) dominated the areas with lower elevations and

were adjacent to the tidal creek. Areas of tall *S. alterniflora* in the southeast of the footprint showed less intra-annual variations over the study period. Despite spatiotemporal variations across the marsh forms, the predicted φPSII exhibited seasonal patterns, with an overall increase from April to June and a local maximum in August. Declines gradually occurred in September and October.

4.15. The Influence of Tide on Predicted PSII Working Efficiency

To investigate seasonal changes of φPSII across the day and tidal conditions, we calculated monthly means of φPSII at three different parts of the day (Morning, noon, and evening) under dry (WT = 0) and flooded (WT > 0) tide conditions for the entire flux tower footprint (Figure 4.11). A two-hour time window was selected for each time period. For example, morning refers to 2 hours after sunrise (PAR > 0), and evening refers to 2 hours before sunset (PAR > 0). Noon indicates daytime between 11:00 and 13:00. Midday monthly mean PSII prediction was always the lowest in each month, and the month-to-month variation was also relatively small within the range of 0.3-0.35. The minimums occur in summer (July and August), with a little above 0.3 in dry conditions and a little below 0.3 in flooded conditions. Springtime PSII predictions were generally higher than summer but very similar to autumn. This suggests that high solar radiation and heat in summer suppress the photosynthetic efficiency of salt marshes regardless of tidal conditions. In addition, predicted PSII is lower under tidal flooding than without flooding at noon during the summertime. These differences were notable in July, when the exceptionally high tide intensities led to additional stress and a decline of *S. alterniflora* photosynthesis when it was already saturated under solar radiation and heat stressors. Conversely, *S. alterniflora* generally had similar photosynthetic efficiency in late spring (April, May) and fall (October), regardless of tidal flooding conditions. This is likely due to the lower

magnitude of environmental stressors and inundation intensity (i.e., dry months) during spring and fall, especially in high-elevation marsh interior areas, which resulted in less noticeable photosynthesis fluctuations.

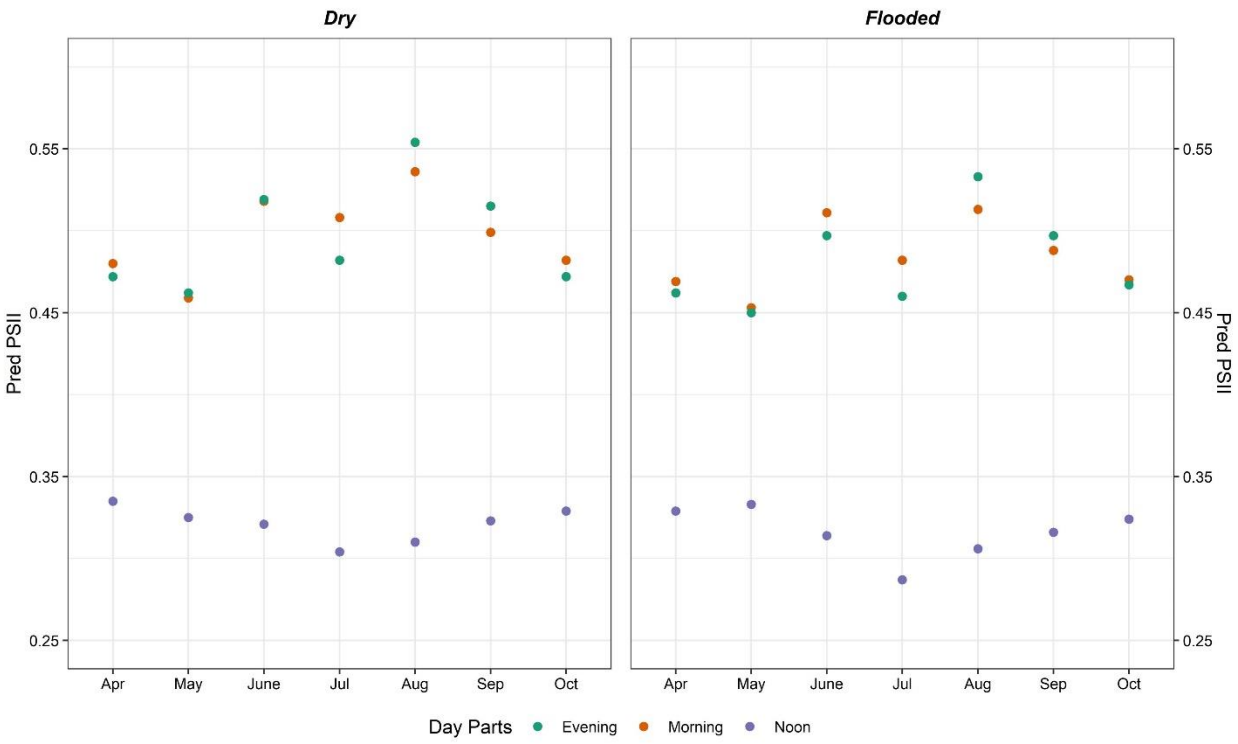

Figure 4.11 Averaged monthly PSII predictions from our random forest model for non-flooded (WT = 0) and flooded (WT > 0) conditions at different parts of the day (Morning; Noon; and Evening) throughout the study period.

Averaged PSII predictions for morning and evening were always higher than noon in the range between 0.45 and 0.55. The monthly variation showed different patterns across the day. For example, morning and evening PSII had an overall increase from late spring to summer and started reducing from late summer, with maximums in August and minimums during spring (Apr, May). Noon shows an opposite trend, with gradual reductions from spring to summer and recoveries from late summer to autumn. Tide flooding did not show significant influences on the

averaged PSII predictions between morning and evening throughout the study period. The month-to-month differences ranged from 1.1% to 5.3% between these two periods. This corresponds to our findings from diurnal PSII variations in section 4.11, i.e., tide flooding has only minimal influences on salt marsh photosynthesis under unstressed environmental conditions.

Reference

Artigas, F., Shin, J. Y., Hobble, C., Marti-Donati, A., Schäfer, K. V., & Pechmann, I. (2015). Long term carbon storage potential and CO2 sink strength of a restored salt marsh in New Jersey. *Agricultural and Forest Meteorology*, 200, 313-321.

Baker, N. R. (2008). Chlorophyll Fluorescence: A Probe of Photosynthesis In Vivo. *Annual Review of Plant Biology, 59*(1), 89-113. doi:10.1146/annurev.arplant.59.032607.092759

Bilger, W., Schreiber, U., & Bock, M. (1995). Determination of the quantum efficiency of photosystem II and of non-photochemical quenching of chlorophyll fluorescence in the field. *Oecologia, 102*(4), 425-432. doi:10.1007/BF00341354

Björkman, O., & Demmig, B. (1987). Photon yield of O2 evolution and chlorophyll fluorescence characteristics at 77 K among vascular plants of diverse origins. *Planta, 170*(4), 489-504. doi:10.1007/BF00402983

Heinsch, F. A., Heilman, J. L., McInnes, K. J., Cobos, D. R., Zuberer, D. A., & Roelke, D. L. (2004). Carbon dioxide exchange in a high marsh on the Texas Gulf Coast: effects of freshwater availability. *Agricultural and Forest Meteorology, 125*(1), 159-172. doi:https://doi.org/10.1016/j.agrformet.2004.02.007

Huang, Y., Chen, Z., Tian, B., Zhou, C., Wang, J., Ge, Z., & Tang, J. (2020). Tidal effects on ecosystem CO2 exchange in a Phragmites salt marsh of an intertidal shoal. *Agricultural and Forest Meteorology, 292*, 108108.

Kathilankal, J. C., Mozdzer, T. J., Fuentes, J. D., D'Odorico, P., McGlathery, K. J., & Zieman, J. C. (2008). Tidal influences on carbon assimilation by a salt marsh. *Environmental Research Letters, 3*(4), 044010. doi:10.1088/1748-9326/3/4/044010

Knox, S. H., Windham-Myers, L., Anderson, F., Sturtevant, C., & Bergamaschi, B. (2018).

Direct and Indirect Effects of Tides on Ecosystem-Scale CO2 Exchange in a Brackish Tidal Marsh in Northern California. *Journal of Geophysical Research: Biogeosciences, 123*(3), 787-806. doi:https://doi.org/10.1002/2017JG004048

Maguire, A. J., Eitel, J. U. H., Griffin, K. L., Magney, T. S., Long, R. A., Vierling, L. A., . . . Bruner, S. G. (2020). On the Functional Relationship Between Fluorescence and Photochemical Yields in Complex Evergreen Needleleaf Canopies. *Geophysical Research Letters, 47*(9), e2020GL087858. doi:https://doi.org/10.1029/2020GL087858

Maxwell, K., & Johnson, G. N. (2000). Chlorophyll fluorescence—a practical guide. *Journal of experimental botany, 51*(345), 659-668.

Murchie, E. H., & Lawson, T. (2013). Chlorophyll fluorescence analysis: a guide to good practice and understanding some new applications. *Journal of Experimental Botany, 64*(13), 3983-3998. doi:10.1093/jxb/ert208

Porcar-Castell, A. (2011). A high-resolution portrait of the annual dynamics of photochemical and non-photochemical quenching in needles of Pinus sylvestris. *Physiologia Plantarum, 143*(2), 139-153. doi:https://doi.org/10.1111/j.1399-3054.2011.01488.x

Porcar-Castell, A., Pfündel, E., Korhonen, J. F. J., & Juurola, E. (2008). A new monitoring PAM fluorometer (MONI-PAM) to study the short- and long-term acclimation of photosystem II in field conditions. *Photosynthesis research, 96*(2), 173-179. doi:10.1007/s11120-008-9292-3

Yang, H., Yang, X., Zhang, Y., Heskel, M. A., Lu, X., Munger, J. W., . . . Tang, J. (2017). Chlorophyll fluorescence tracks seasonal variations of photosynthesis from leaf to canopy in a temperate forest. *Global Change Biology, 23*(7), 2874-2886. doi:https://doi.org/10.1111/gcb.13590

Chapter 5:

DISCUSSION

5.1. PSII Working Efficiency is Significantly Reduced in Submerged Canopies

We observed up to 41% reduction in φPSII when BOC leaves were fully submerged (Table 4.2). Reductions in φPSII began when tide height approached 30 cm, 5 cm below the BOC sensor (Figure 4.4a). Additionally, NPQ dropped rapidly to near 0 accompanied by simultaneously increased fluorescence yields when leaves were fully submerged by tides > 35 cm (BOC sensor height). This indicated that most of the APAR may have been lost as fluorescence in underwater leaves. We attribute this to the decrease in the fraction of 'open' PSII reaction centers and the stomatal conductance rate during submergence (Figure 5.1). Our novel findings quantitatively relate φPSII reduction in fully submerged leaves to the physiological characteristics of *S. alterniflora* canopies in field settings, although similar observations were reported in laboratory experiments by Pezeshki et al. (1993). The closures of PSII reaction centers and stomata are likely what eventually led to decreases in CO_2 assimilation rates and light use efficiency (LUE) in *S. alterniflora* during tidal flooding, as observed by Nahrawi et al. (2020) and Hawman et al. (2021).

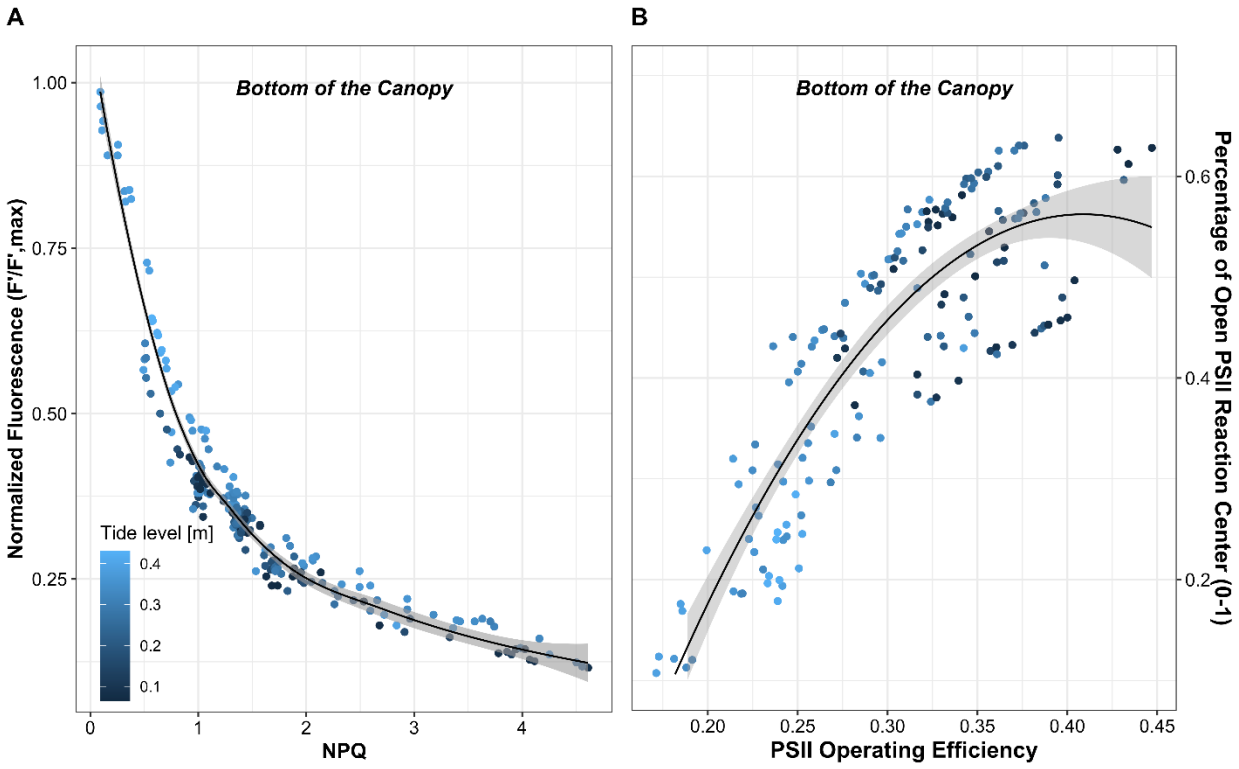

Figure 5.1 Analysis of chlorophyll fluorescence (ChlF) parameters at bottom (BOC) of the *S. alterniflora* canopy during midday (local time 10:00 – 16:00) and high tidal flooding. (a) Relationship between steady-state fluorescence yield (F′) and non-photochemical quenching (NPQ). (b) relationship between the fraction of "open" PSII reaction centers (qL) and quantum efficiency of PSII (φPSII) for BOC *S. alterniflora* leaves. Lighter blue points indicate a higher tide level above the soil surface. In (a), a low NPQ and high fluorescence yield is observed during high tide level. In (b) underwater photochemistry was observed at a greatly reduced rate accompanied by partially opened PSII reaction centers during high tidal flooding. The φPSII and qL are also positively associated. Polynomial smoothing lines with 95% confidence intervals (grey areas) were fitted for trend visualization purposes. Observations of F' were normalized to the maximum in the light (F', max) following Magney et al. (2017).

5.2. Photosynthetic Activities were Observed in Fully Submerged Canopies

Despite the sharp decline in photosynthetic activities, our results suggest that fully submerged leaves at the bottom of the *S. alterniflora* canopy continued to photosynthesize during high flooding because a small proportion of PSII reaction centers remained partially open. Figure 6b shows at least 10% of PSII reaction centers in BOC *S. alterniflora* leaf carried out photochemistry at 20% capacity under complete submergence compared to air-exposed conditions. Previous studies observed similar phenomena in Virginia tidal marshes, where *S. alterniflora* continued to photosynthesize under tidal inundation (Kathilankal et al., 2008). Kathilankal et al. (2008) measured an average 66% reduction in relative electron transport rate (rETR) for submerged leaves. We observed a similar but lower reduction (41%) in BOC φPSII, which is directly proportional to rETR, when the sensor and leaf were fully submerged (Table 4.2b). This difference could be attributed to actual flooding depth, differential attenuation of PAR in the water column, or differences in flooding duration. Additionally, canopy morphology could also affect photosynthetic rates at different heights within the canopy. In our GA study, our plant height was almost twice the height of plants at their VA site (110 ± 2.3 cm compared to 62.6 ± 1.9 cm).

5.3. PSII Working Efficiency in Air-exposed Canopy is Largely Unaffected by Submerged Bottom Canopy

Our results showed that TOC air-exposed leaves only had small reductions in φPSII (6.3-8.3%) during tidal flooding and only a negligible difference (0.7%) when the tide height rose above 35 cm (Table 4.2). Additionally, there were no clear relationships between TOC φPSII and incoming tide (tide in) or outgoing tide (tide out) periods (Figure 4.3b and Figure 4.4b). Kathilankel et al. (2008) demonstrated reductions in the photosynthetic ability of submerged leaves, however, it is unclear if their comparison is to air-exposed leaves during partial

submergence or to dry conditions during non-flooding conditions. Our results clearly indicated air-exposed leaves experienced little reductions in φPSII when, concurrently, the lower leaves submerged by tidal waters had reduced φPSII. Therefore, we conclude that photosynthesis in TOC and BOC leaves are independent of each other, and reductions from tidal flooding only occur when leaves are actively submerged. Further, our study shows that as flood water depth increases, φPSII decreases (Figure 4.4a). When considering the φPSII of the entire canopy as a whole, a 25 cm tide height would lead to a 23.3% decrease in φPSII, while a 45 cm tide height would double the φPSII reduction (48%). These estimates are derived from plant-level φPSII decreases observed by the combined TOC and BOC sensors during flooded conditions compared to non-flooded conditions (Tables 4.2). This highlights extra complexities involved in understanding the photosynthetic processes across *S. alterniflora* canopies under different tide ranges. Our ChlF measurements at the bottom and top of the same plant canopy showed independent and different light and temperature (heat) responses of plant metabolism, which were closely linked to inundation status. It also provides new insights into estimating the efficiency of energy partitioning of *S. alterniflora* PSII at different canopy positions during tidal flooding as a consequence of changes in the proportion of submerged/emergent leaves.

5.4. Impacts of PSII Working Efficiency Variations during Tidal Flooding on Canopy Scale Studies

The impact of flooding on leaf-level photosynthesis is driven by submergence status, as discussed in section 5.1. Therefore, the proportion of tide:plant height is a significant variable in estimating photochemical efficiency at the canopy scale (e.g. ‘see section 5.3’). Although not the same type of measurements, our findings are aligned with data presented by many previous studies on the influence of tidal flooding on CO_2 fluxes or net ecosystem exchange (NEE) or

GPP, which have shown decreases in marsh carbon exchange under tidal inundation at ecosystem-scale. For example, Moffett et al. (2010) found a substantial decrease in CO_2 fluxes for *S. alterniflora* in a California marsh when the tide depth exceeded 17 cm above the ground. Forbrich & Giblin (2015) showed a tide depth above 5 cm could lead to a reduction in marsh productivity. We could not find any study linking in-situ ChlF to CO_2 fluxes or Eddy tower scale NEE or GPP for wetlands. It may likely be due to various challenges involved in continuously capturing leaf-level φPSII variations at different plant heights under realistic field tidal inundation. But, we can assume that the variability in in-situ ChlF due to tidal inundation would have an impact on CO_2 fluxes or GPP because many prior studies have shown ChlF as a strong indicator of seasonal variability and phenology of GPP in other terrestrial vegetative ecosystems (Flexas et al., 2002; Joiner et al., 2013).

However, our findings bring new complexities to studies involving passive measurements of photosynthesis proxies (e.g., SIF) or carbon assimilation rates (e.g., NEE and GPP via Eddy flux tower). We lack evidence to suggest that ongoing and reduced photosynthesis in fully submerged *S. alterniflora* leaves is directly linked to active gas exchange underwater. This link is needed because we do not know whether marsh species such as *S. alterniflora* internally recycle CO_2 and O_2 (Gleason & Dunn, 1981) produced through photosynthesis, photorespiration, and respiration; or whether they significantly exchange gases with the water column while submerged (Silva et al., 2005; Winkel et al., 2011); A combination of the two phenomena is also possible. Once these uncertainties are better understood, we expect methodological revisions will be necessary for canopy scale NEE calculations and partitioning models (i.e., submerged vs. emergent canopies) to estimate GPP and ecosystem respiration for tidal wetlands. These new

methods would need to quantify canopy submergence and link it with augmented rates of photosynthesis and gas exchange during tidal flooding.

5.5. Advantages of Active PSII Working Efficiency Measured at Leaf-Level

There are several advantages associated with PAM fluorometry-based ChlF data to further understand the dynamics and drivers of underwater canopy photosynthesis. First, PAM fluorometry can be designed for long-term, continuous deployment. This allows for reliable measurements of maximal and minimal levels of ChlF when the photosynthetic apparatus is fully relaxed under field conditions at night. Accurate field-based determination of F0 and Fm allows for the quantification of NPQ, Fv/Fm, and photochemical quenching (PQ), which are normally difficult to acquire. Second, PAM fluorometers can be deployed and collect data under complicated field conditions, such as in tidal wetlands with soft ground and saturated soils. Third, PAM MONI – HEAD/S observe the same set of leaves and move together with them, which allows for consistent measurements and interpretations throughout the entire monitoring period. Fourth, the monitoring PAM fluorometer can connect up to 7 measuring heads capable of measuring ChlF independently. Our deployment system design can not only provide average measurements across multiple stems that allow the analysis of ChlF variations within complex canopy structures, but also provide more measuring points on a larger scale which could be comparable to a flux tower footprint or MODIS 500-m pixel to develop empirical relationships. This will be particularly useful in scaling up leaf-level photosynthesis variations within flux tower footprints and connecting to satellite measurements at larger spatial scales.

5.6. Application of Active PSII Working Efficiency Measurements

Our controlled *in situ* measurements of leaf-scale ChlF provide fundamental information that can explain vertical changes in the PSII working mechanism. These results suggested that in order to better understand the photosynthesis and carbon assimilation rates (e.g., GPP) of salt marshes that are frequently inundated, it is essential to understand how changes in in-situ photochemical activities are affected by tide-induced submergence of leaf area. If such empirical relationships between ChlF parameters representing photochemistry and GPP can be established in future studies, it can further our understanding of fluctuations of photosynthesis, SIF spectral shapes, and GPP in salt marshes observed during tidal flooding at multiple scales. In this context, our method can be coupled with gas exchange measurements from Eddy covariance flux towers or radiant retrieval of ChlF from passive sensors (e.g., SIF). That would allow for further assessment of the influence of tidal inundation on marsh photosynthesis and how it affects carbon flux budgets at larger scales. Hawman et al. (2021) showed environmental factors, including air temperature, vapor pressure deficits, solar radiation, and tides affect LUE and GPP of *S. alterniflora*. All of those environmental variables could also be used in future studies to model and predict φPSII for marsh canopies so that φPSII predictions can be scaled to sites where in-situ ChlF measurements are unavailable. Future studies should also examine these phenomena in marshes dominated by other common species, such as *J. roemerianus* and *S. patens*, which respond to similar environmental gradients.

5.7. Limitation of PSII Working Efficiency Measured at Leaf-Level during Tidal Inundation

Our observations of the tidal flooding impacts on φPSII, whether during low tide or high tide, is limited by sensor reliability, sensor deployment height, and the maximum tide height during the study period, which did not exceed 45 cm above the soil surface. Tides that submerge

TOC leaves are not frequent in our study marsh (Hawman et al., 2021; O'Connell et al., 2017). We anticipate that the whole plant φPSII reductions will increase once a threshold flooding level is exceeded because TOC φPSII will have a greater reduction, particularly when it becomes partially or fully submerged. Therefore, more data measuring the vertical distribution of photosynthetic efficiency through φPSII measurements at varying canopy heights would help in developing a method to estimate canopy-scale marsh photosynthetic efficiency. However, the conditions during the study were representative of the most typical flood patterns at our site. Our observations suggest that photosynthetic efficiency does not change significantly as long as the majority of the canopy is air-exposed during low-level tidal flooding.

5.8. Difference in the influence of Tide on predicted PSII working efficiency across time

The effects of tidal flooding on the variation of predicted PSII were examined over the course of a day and throughout the season. We found that PSII prediction is affected by tidal flooding. The tidal effects on the PSII predictions throughout plant physiology was quantified by comparing the difference in the PSII during the tidal flooded and non-flooded periods. The tide significantly reduced the diurnal PSII by 20.5% and averaged monthly PSII by up to 8.7% in summertime. This is consistent with the previous findings for this species that the tidal flooding led to the diminished opening of PSII reaction centers and reduced stomatal conductance rate (Kathilankal et al., 2008; Mao et al., in press, 2023). These physiological changes induced by tidal inundation ultimately result in lower photosynthetic activity in *S. alterniflora* because the electron transport rate (light reaction) and carbon assimilation (dark reaction) are coordinated in C4 plants (Genty et al., 1989). Therefore, changes in environmental conditions, including tidal flooding, can regulate and track the efficiency with which a photon is used to drive photosynthesis. At the seasonal time scale, the influence of WT on PSII was the highest in

August, and it was twice as strong as in spring months (Figure 4.11), implying that photosynthetic activities fluctuated more with high tide depth and long-duration tides (Figure 4.6). This indicates that longer and higher tidal flooding results in larger reductions in productivity (Huang et al., 2020), which is also consistent with the suppression of daytime NEE induced by tides reported in previous studies (Forbrich and Giblin, 2015; Kathilankal et al., 2008 Moffett et al., 2010; Nahrawi et al., 2020).

5.9. The Contributions of Tide Inundation to the Predictions of PSII Working Efficiency

Tide shows significant impact on the φPSII across time scales, and it was an important variable in our random forest model. Although not the same type of models, our variable importance is aligned with the model presented by previous studies on the influence of tidal flooding on salt marsh light use efficiency (LUE) or net ecosystem exchange (NEE), which have shown decreases in Spartina LUE and carbon exchange under tidal inundation. For example, Hawman et al. (2020) found tide was the most important parameter that contributed 58.2% changes in explained deviance for the generalized additive model (GAM) based LUE prediction for Spartina marsh. However, WT only accounts for ~ 20% changes in our model accuracy. We attribute the lower importance of WT in our model to environmental, morphological, and physiological factors. First, our study site tended to be inundated by short duration tides with low tidal depths. In particular, during the midday, tidal flooding exceeding 0.3m above the marsh surface occurred only 8 times during the entire 36 days sampling period (5 days in 2020 plus 3 days in 2018) in our study site (Figure 4.6). Low tidal flooding reduced the duration of the tidal water flooding during the daytime, which diminished the importance of tide in our model. Correspondingly, Hawman *et al*. (2020) observed high tide intensities (>0.5 m flooding above

the soil surface in up to 19 days per month) during their study period. The differences in flooding frequency and magnitude could have led to the lower importance of WT on the model outcome. Second, our predicted φPSII is modeled for leaves at the top of the canopy, which was never submerged during our experiment. The exposed part of the plant continued photosynthesizing at slightly reduced rate (7 - 8.3% reduction) when the bottom of the canopy is inundated by tide flooding (Mao et al., in press, 2023). Therefore, the responses of PSII physiological processes (NIRV, see section 4.12) is more impactful than the WT in φPSII prediction (Figure 4.9). Third, further analysis by time shows that WT and related variables (e.g., Tsoil) become drivers of the predicted φPSII when it is saturated at midday. We theorize that the changes in WT and corresponding changes in Tsoil and Tair would have increased impacts on the φPSII prediction if a higher percentage of salt marshes is inundated with longer inundation duration. In this context, our random forest model should have shown the realistic response of TOC φPSII to tidal inundation.

5.10. Advantages of Ground-Based PSII Working Efficiency Model

To the best of our knowledge, this is the first bottom-up model that uses continuous field measurements to understand the relationship between φPSII and environmental variables in *S. alterniflora*, and especially that also accounts for the influence of regular flooding by tide. There are several advantages associated with our ChlF model compared to the traditional spectrum-based solar induced fluorescence (SIF) models for photosynthetic research in tidal wetlands. First, our PSII predictions were able to track instantaneous changes in photosynthesis at a finer spatial scale over the short time scale because ChlF is much more responsive to PAR than SIF (Gu et al., 2019). This is due to the fact that ChlF contains direct and valuable physiological information revealing the probability of absorbed light energy will be used for photochemistry.

This high sensitivity to light levels of ChlF is crucial for studying diurnal variations in plant photosynthesis because it is unlikely that GPP saturation is constant across time, species, and location. SIF, on the other hand, is highly correlated with APAR, which diminishes its ability to show changes from the saturating light response of photosynthesis over shorter times. Therefore, it only acts as a "proxy" for photosynthesis over longer time scales or from coarse spatial resolution (Frankenberg et al., 2011; Guan et al., 2016; Guanter et al., 2014; Joiner et al., 2011; Sun et al., 2017).

Second, our predicted PSII reflects the variation of photosynthesis during environmental stress (e.g., tide, high temperature, and radiation) under natural conditions due to changes in plant biophysical processes. This matches with previous studies about photosynthesis variations on the diurnal to seasonal scale in response to environmental gradients. For example, NPQ increases with increased PAR (Baker, 2008), the fraction of 'open' PSII reaction centers "qL" decreases with increased tidal flooding (Mao et al., in press, 2023), reductions in stomatal conductance are also observed during drought (Helm et al., 2020). However, passive ChlF measurements are weak at tracking variations of photosynthesis at the physiological level for most ecosystems because it only mirrors change as a function of APAR (Magney et al., 2020)

Third, our predicted PSII is more consistent because it is less affected by meteorological conditions and morphological differences in canopies. In contrast, spatial and temporal variations in vegetation structure influence remote sensed ChlF observations (i.e., SIF) on the diurnal to the seasonal scales because the amount of SIF photons reaching the sensor is altered by the angle of light incidence (Chang et al., 2020), light intensity and cloudiness (Grossmann et al., 2018), leaf density and thickness (Wittenberghe et al., 2015) as well as sensor viewing geometry (Joiner et al., 2020). Therefore, the bottom-up ChlF model can simplify the uncertainties associated with

SIF-based estimations by relating plant photosynthesis with common environmental variables that are widely available and easily retrieved from multiple platforms at various spatial and temporal scales. This also reduces the complexity and cost of measuring and predicting canopy structural parameters for the interpretation of SIF via remote sensing.

5.11. Limitation of PSII Working Efficiency Prediction

There are a few limitations to be recognized in our model. First, our φPSII predictions were limited to the top of the *S. alterniflora* canopy, which never became fully submerged during our sampling period due to the low tidal flooding (section 5.8). This affects our predictions of photosynthetic efficiency during tidal flooding. Second, the entire ChlF dataset was limited to the summertime after data cleaning and filtering. This reduces the temporal compatibility of our model because input parameters may be out of the range with respect to the training dataset used in our model. For example, predicted monthly PSII in early spring (e.g., April) are homogeneous with less spatial variations compared to summer predictions.

5.12. Possible Improvements for Future PSII Working Efficiency Modeling

Future studies can deploy separate sensors at different canopy levels to quantify the vertical variations of photosynthesis within the canopy. For example, there were studies deploying multiple quantum sensors to investigate the relationship between crop photosynthesis and light profile within the canopy (Li & Yang, 2015). This vertical profile of the solar radiation and ChlF emissions within the canopy can also reveal the underlying mechanism that controls the plant's physiological process when it is under various flooding depths, including the rate of PQ (e.g., stomata openness & stomatal conductance), NPQ (heat dissipation), and availability of CO_2 and solar radiation varies under different inundation status (e.g., fully submerged vs.

partially submerged) (Mao et al., in press, 2023; Gu et al., 2019). This would eventually lead to a better understanding of the spatiotemporal relationships between photosynthesis and GPP as the magnitude of tidal suppression on GPP is controversial in salt marshes reported by previous studies (Forbrich and Giblin, 2015; Kathilankal et al., 2008; Knox et al., 2018; Li et al., 2014; Moffett et al., 2010). In addition, future studies can include more variables, such as wind direction and salinity, which have also been demonstrated to influence the photosynthetic activities on salt marshes (Huang et al., 2022). However, the ideas listed above require more complex data collection design, for example, separate quantum sensors and fluorometers across canopy heights. The aspects of more comprehensive data collection research are important but beyond the scope of this dissertation.

In addition, future studies can extend the data sampling period to improve the range of ChlF parameters. However, continuous, accurate, and reliable measurements of ChlF emission in coastal environment as well as across canopy types remains difficult and challenging despite efforts in frame design, sensor preprograming, and maintenance (Logan et al., 2007; Magney et al., 2017; Mao et al., in press, 2023). This is mainly due to the limitations of hardware equipment, as the current sensors are generally more reliable in terrestrial ecosystems. For example, PAM fluorometry is well utilized over broadleaf (Lysenko et al., 2020), while using it in salt marshes, such as *S. alterniflora* in our study, remains challenging because multiple thin *S. alterniflora* leaves are needed to fill the PAM sampler. This often results in the leaves overlapping in the sampler and affects the reliability of ChlF observations (Mao et al., in press, 2023). Frequent field visits are also recommended to clean the sensor and make sure the monitored leaves remain healthy although measurement without cleaning does reflect realistic field conditions. Addressing these challenges can facilitate the continuous and reliable

measurements of highly dynamic leaf ChlF measurements in future studies, which will, in particular, help scale our model to other regions with different environmental and tidal conditions.

Third, the estimated ChlF using the method proposed in this study needs to be validated. Magney et al. (2017) demonstrated an instrument that could measure leaf-level gas exchange simultaneously with PAM ChlF, PAR, and spectrally resolved fluorescence. Such systems can be modified to quantify the effects of tidal flooding on plant productivity and investigate the relationship between ChlF and leaf-level gas exchange across a range of temporal scales, and vertical gradients within the canopy. Unmanned aircraft systems (UAS) can provide on-demand and non-destructive ChlF measurements at high spatial resolutions, but to the best of our knowledge, such systems have not emerged for fluorescence measurements in frequently flooded marsh ecosystems (Bendig et al., 2018; Mac Arthur et al., 2014). We assume that the development of UAV-based ChlF system could significantly improve the understanding of the diurnal relationship between plant photosynthesis and environmental conditions under tidal flooding because it will able to capture the high variability in stressed vegetation, and it can also serve as an intermediate information layer between in-situ and satellite sensors, with the advantage of higher spatial resolution between leaf-level and canopy scale GPP estimated from EC tower-based CO_2 flux exchange. Integrating this with the bottom-up ChlF model developed in this study can potentially lead to novel research studies investigating spatiotemporal variations of photosynthesis in salt marshes.

Reference

Baker, N. R. (2008). Chlorophyll Fluorescence: A Probe of Photosynthesis In Vivo. *Annual Review of Plant Biology, 59*(1), 89-113. doi:10.1146/annurev.arplant.59.032607.092759

Bendig, J., Gautam, D., Malenovský, Z., & Lucieer, A. (2018, July). Influence of cosine corrector and UAS platform dynamics on airborne spectral irradiance measurements. In *IGARSS 2018-2018 IEEE International Geoscience and Remote Sensing Symposium* (pp. 8822-8825). IEEE.

Chang, C. Y., Guanter, L., Frankenberg, C., Köhler, P., Gu, L., Magney, T. S., ... & Sun, Y. (2020). Systematic assessment of retrieval methods for canopy far-red solar-induced chlorophyll fluorescence using high-frequency automated field spectroscopy. *Journal of Geophysical Research: Biogeosciences*, 125(7), e2019JG005533.

Feagin, R. A., Forbrich, I., Huff, T. P., Barr, J. G., Ruiz-Plancarte, J., Fuentes, J. D., ... & Miao, G. (2020). Tidal wetland gross primary production across the continental United States, 2000–2019. *Global Biogeochemical Cycles, 34*(2), e2019GB006349.

Flexas, J., Bota, J., Escalona, J., Sampol, B., & Medrano, H. (2002). Effects of drought on photosynthesis in grapevines under field conditions: An evaluation of stomatal and mesophyll limitations. *Functional Plant Biology - FUNCT PLANT BIOL, 29*. doi:10.1071/PP01119

Forbrich, I., & Giblin, A. E. (2015). Marsh-atmosphere CO2 exchange in a New England salt marsh. *Journal of Geophysical Research: Biogeosciences, 120*(9), 1825-1838. doi:https://doi.org/10.1002/2015JG003044

Frankenberg C, Fisher JB, Worden J, Badgley G, Saatchi SS, Lee JE, Toon GC, Butz A, Jung M, Kuze A *et al*. 2011. New global observations of the terrestrial carbon cycle from

GOSAT: patterns of plant fluorescence with gross primary productivity. *Geophysical Research Letters* **38**: L17706.

Genty, B., Briantais, J.-M., & Baker, N. R. (1989). The relationship between the quantum yield of photosynthetic electron transport and quenching of chlorophyll fluorescence. *Biochimica et Biophysica Acta (BBA) - General Subjects, 990*(1), 87-92. doi:https://doi.org/10.1016/S0304-4165(89)80016-9

Gleason, M. L., & Zieman, J. C. (1981). Influence of tidal inundation on internal oxygen supply of Spartina alterniflora and Spartina patens. *Estuarine, Coastal and Shelf Science, 13*(1), 47-57. doi:https://doi.org/10.1016/S0302-3524(81)80104-1

Grossmann, K., Frankenberg, C., Magney, T. S., Hurlock, S. C., Seibt, U., & Stutz, J. (2018). PhotoSpec: A new instrument to measure spatially distributed red and far-red solar-induced chlorophyll fluorescence. *Remote Sensing of Environment*, **216**, 311– 327. https://doi.org/10.1016/j.rse.2018.07.002

Gu, L., Han, J., Wood, J. D., Chang, C. Y. Y., & Sun, Y. (2019). Sun-induced Chl fluorescence and its importance for biophysical modeling of photosynthesis based on light reactions. *New Phytologist*, *223*(3), 1179-1191.

Guan K, Berry JA, Zhang Y, Joiner J, Guanter L, Badgley G, Lobell DB. 2016. Improving the monitoring of crop productivity using spaceborne solar-induced fluorescence. *Global Change Biology* **22**: 716– 726.

Guanter L, Zhang Y, Jung M, Joiner J, Voigt M, Berry JA, Frankenberg C, Huete AR, Zarco-Tejada P, Lee J-E *et al*. 2014. Global and time-resolved monitoring of crop photosynthesis with chlorophyll fluorescence. *Proceedings of National Academy of Sciences, USA* **111**: E1327– E1333.

Hawman, P. A., Mishra, D. R., O'Connell, J. L., Cotten, D. L., Narron, C. R., & Mao, L. (2021). Salt Marsh Light Use Efficiency is Driven by Environmental Gradients and Species-Specific Physiology and Morphology. *Journal of Geophysical Research: Biogeosciences, 126*(5), e2020JG006213. doi:https://doi.org/10.1029/2020JG006213

Helm, L. T., Shi, H., Lerdau, M. T., & Yang, X. (2020). Solar-induced chlorophyll fluorescence and short-term photosynthetic response to drought. *Ecological Applications*, *30*(5), e02101.

Huang, Y., Chen, Z., Tian, B., Zhou, C., Wang, J., Ge, Z., & Tang, J. (2020). Tidal effects on ecosystem CO2 exchange in a Phragmites salt marsh of an intertidal shoal. *Agricultural and Forest Meteorology*, *292*, 108108.

Huang, Y., Zhou, C., Du, M., Wu, P., Yuan, L., & Tang, J. (2022). Tidal influence on the relationship between solar-induced chlorophyll fluorescence and canopy photosynthesis in a coastal salt marsh. *Remote Sensing of Environment*, *270*, 112865. Doi: https://doi.org/10.1016/j.rse.2021.112865

Joiner, J., Guanter, L., Lindstrot, R., Voigt, M., Vasilkov, A. P., Middleton, E. M., . . . Frankenberg, C. (2013). Global monitoring of terrestrial chlorophyll fluorescence from moderate-spectral-resolution near-infrared satellite measurements: methodology, simulations, and application to GOME-2. *Atmos. Meas. Tech., 6*(10), 2803-2823. doi:10.5194/amt-6-2803-2013

Joiner, J., Yoshida, Y., Köehler, P., Campbell, P., Frankenberg, C., van der Tol, C., Yang, P., Parazoo, N., Guanter, L., & Sun, Y. (2020). Systematic orbital geometry-dependent variations in satellite solar-induced fluorescence (SIF) retrievals. *Remote Sensing*, **12**, 2346. https://doi.org/10.3390/rs12152346

Joiner, J., Yoshida, Y., Vasilkov, A. P., & Middleton, E. M. (2011). First observations of global and seasonal terrestrial chlorophyll fluorescence from space. *Biogeosciences, 8*(3), 637-651

Kathilankal, J. C., Mozdzer, T. J., Fuentes, J. D., D'Odorico, P., McGlathery, K. J., & Zieman, J. C. (2008). Tidal influences on carbon assimilation by a salt marsh. *Environmental Research Letters, 3*(4), 044010. doi:10.1088/1748-9326/3/4/044010

Knox, S. H., Windham-Myers, L., Anderson, F., Sturtevant, C., & Bergamaschi, B. (2018). Direct and Indirect Effects of Tides on Ecosystem-Scale CO2 Exchange in a Brackish Tidal Marsh in Northern California. *Journal of Geophysical Research: Biogeosciences, 123*(3), 787-806. doi:https://doi.org/10.1002/2017JG004048

Li, T., & Yang, Q. (2015). Advantages of diffuse light for horticultural production and perspectives for further research. *Frontiers in Plant Science*, 6, 704

Logan, B., Adams, W., & Demmig-Adams, B. (2007). Viewpoint: Avoiding common pitfalls of chlorophyll fluorescence analysis under field conditions. *Functional Plant Biology - FUNCT PLANT BIOL, 34*. doi:10.1071/FP07113

Lysenko, V., Guo, Y., Kosolapov, A., Usova, E., Varduny, T., & Krasnov, V. (2020). Polychromatic Fourier-PAM fluorometry and hyperspectral analysis of chlorophyll fluorescence from Phaseolus vulgaris leaves: Effects of green light. Information Processing in Agriculture, 7(2), 204-211.

MacArthur, A., Robinson, I., Rossini, M., Davis, N., & MacDonald, K. (2014). A dual-field-of-view spectrometer system for reflectance and fluorescence measurements (Piccolo Doppio) and correction of etaloning. In *Fifth International Workshop on Remote Sensing of Vegetation Fluorescence*. European Space Agenccy.

Magney, T. S., Barnes, M. L., & Yang, X. (2020). On the covariation of chlorophyll fluorescence and photosynthesis across scales. *Geophysical Research Letters, 47*(23), e2020GL091098.

Magney, T. S., Frankenberg, C., Fisher, J. B., Sun, Y., North, G. B., Davis, T. S., . . . Siebke, K. (2017). Connecting active to passive fluorescence with photosynthesis: a method for evaluating remote sensing measurements of Chl fluorescence. *New Phytologist, 215*(4), 1594-1608. doi:https://doi.org/10.1111/nph.14662

Mao, L, Mishra, D. R., Hawman, P. A., Narron, C. R., O'Connell, J. L., & Cotten, D. L. (in press). Photosynthetic Performance of Tidally Flooded Spartina alterniflora Salt Marshes. *Journal of Geophysical Research: Biogeosciences*

Moffett, K. B., Wolf, A., Berry, J. A., & Gorelick, S. M. (2010). Salt marsh–atmosphere exchange of energy, water vapor, and carbon dioxide: Effects of tidal flooding and biophysical controls. *Water Resources Research, 46*(10).

Nahrawi, H., Leclerc, M. Y., Pennings, S., Zhang, G., Singh, N., & Pahari, R. (2020). Impact of tidal inundation on the net ecosystem exchange in daytime conditions in a salt marsh. *Agricultural and Forest Meteorology, 294*, 108133

O'Connell, J. L., Mishra, D. R., Cotten, D. L., Wang, L., & Alber, M. (2017). The Tidal Marsh Inundation Index (TMII): An inundation filter to flag flooded pixels and improve MODIS tidal marsh vegetation time-series analysis. *Remote Sensing of Environment, 201*, 34-46. doi:https://doi.org/10.1016/j.rse.2017.08.008

Pezeshki, S. R., Pardue, J. H., & Delaune, R. D. (1993). The influence of soil oxygen deficiency on alcohol dehydrogenase activity, root porosity, ethylene production and photosynthesis in Spartina patens. *Environmental and Experimental Botany, 33*(4), 565-573.

doi:https://doi.org/10.1016/0098-8472(93)90031-A

Silva, J., Santos, R., Calleja, M. L., & Duarte, C. M. (2005). Submerged versus air-exposed intertidal macrophyte productivity: from physiological to community-level assessments. *Journal of Experimental Marine Biology and Ecology*, *317*(1), 87-95. doi:https://doi.org/10.1016/j.jembe.2004.11.010

Sun Y, Frankenberg C, Wood JD, Schimel DS, Jung M, Guanter L, Drewry DT, Verma M, Porcar-Castell A, Griffis TJ *et al*. 2017. OCO-2 advances photosynthesis observation from space via solar-induced chlorophyll fluorescence. *Science* **358**: eaam5747.

Tao, J., Mishra, D. R., Cotton, D. L., O'Connell, J., Leclerc, M., Binti Nahrawi, H., et al. (2018). A comparison between the MODIS product (MOD17A2) and a tide-robust empirical GPP model evaluated in a Georgia wetland. *Remote Sensing*, 10, 10.3390.

Van Wittenberghe, S., Alonso, L., Verrelst, J., Moreno, J., & Samson, R. (2015). Bidirectional sun-induced chlorophyll fluorescence emission is influenced by leaf structure and light scattering properties—A bottom-up approach. *Remote Sensing of Environment*, *158*, 169-179.

Winkel, A., Colmer, T. D., & Pedersen, O. L. E. (2011). Leaf gas films of Spartina anglica enhance rhizome and root oxygen during tidal submergence. *Plant, Cell & Environment, 34*(12), 2083-2092. doi:https://doi.org/10.1111/j.1365-3040.2011.02405.x

Chapter 6:

CONCLUSION

We designed and deployed a novel field measuring system that measures high temporal resolution leaf-scale chlorophyll fluorescence, PSII operating efficiency, and light regime in the marsh using pre-programmed pulse-amplitude modulation chlorophyll fluorometer, and underwater quantum sensors. To the best of our knowledge, we are the first to employ these measurements to investigate the photosynthetic response of the dominant salt marsh plant, *S. alterniflora* to tidal inundation in the field condition. We used this novel measuring system in collecting the continuous and high temporal resolution ChlF measurements at the top (~105 cm) and bottom (~35 cm) of the salt marsh *S. alterniflora* canopy. It provides the opportunity to directly monitor and investigate leaf ChlF and photosynthesis at different positions of the *S. alterniflora* canopy under natural field conditions. We observed three stages of diurnal variations of *S. alterniflora* ChlF parameters. Generally, F_m' decreased with a corresponding F' increase after sunrise; they changed in similar patterns during the day, and both started recovery in the early evening with a steady decrease of F' and a constant rise in F_m'. These ChlF variations denoted that salt marsh PSII can rapidly adjust the distribution of the absorbed light energy in response to changes in the natural field condition.

Our leaf-level ChlF measurements, for the first time, also demonstrated the variation of leaf ChlF and photosynthetic activities in air-exposed, partially submerged, and fully submerged Spartina plants across a range of tidal cycles and differing tidal amplitudes. We found the influence of tidal inundation on *S. alterniflora* photosynthetic performance was independent and

different in the leaves across the canopy. The observed differences could be explained by differences in meteorological and physiological stresses between the two sampling locations induced by changes in leaf submergence conditions. For example, φPSII slightly varied at the top and bottom of the canopy comparing to non-flooding condition during low tidal flooding. On days with high tidal flooding, the φPSII of BOC leaves decreased with increasing tide height, the reduction became more pronounced (up to 41%) when the tide height > 35 cm completely submerged BOC leaves compared to non-flooding conditions. However, less than 10% reductions were observed in φPSII of air-exposed leaves at time when the BOC leaves were complete submerged. Additionally, we observed underwater photosynthesis at a greatly reduced rate accompanied by partially opened PSII reaction centers and low NPQ in fully submerged *S. alterniflora* leaves during tidal flooding. We quantified that φPSII of fully submerged *S. alterniflora* leaf was still at 20% capacity compared to air exposed conditions because at least 10% of PSII reaction centers remained open and carried out photochemistry under complete submergence. This suggests that *S. alterniflora* could potentially remain a CO_2 sink during tidal inundation. We concluded that the proportion of plant submergence should be considered a significant parameter in estimating GPP at the canopy scale.

We developed an φPSII prediction model for *S. alterniflora* using biophysical and meteorological variables from GCE-flux tower and from satellite data in a random forest model. We evaluated the model performance and accuracy against our in-situ φPSII measurements. Our model produced reliable results with a root mean square error of 0.9 on the global validation dataset with the observed φPSII ranging from 0.22 and 0.75. Our model also provided evidence demonstrating a relationship between *S. alterniflora* photosynthesis and environmental gradients as the importance of all six variables were explored. In particular, PAR, NIRv, Tsoil, and WT

have significant impacts on the φPSII outcomes of our random forest model. We observed variability in *S. alterniflora* photosynthesis in the prediction map over the growing season across the GCE-Flux tower footprint. We attribute the observed differences to geomorphic and physiological differences. For example, tidal flooding magnitude and canopy height forms varied greatly due to elevation differences. Under the same tidal inundation at 9:00 LST, we observed distinctly different φPSII that could be explained by the proportion of submerged/emergent leaves and flooding tolerances. In addition, our results showed that environmental stressors (i.e., tidal flooding and high light intensity) could cause large fluctuations in diurnal φPSII that may not be captured in more generalized measurement and modeling. It suggests that φPSII should be parameterized bottom-up from local environmental variables with high temporal resolution.

We presented a novel modeling approach that outlines an accurate and low-cost path to predict tidally flooded *S. alterniflora* salt marshes photosynthetic efficiency without having high-resolution ChlF data by utilizing environmental and biophysical variables. The wide availability of such variables, for example, well-established EC flux sites, makes this method replicable to areas with different spatio-temporal scales. Integrating the analytical framework developed in this dissertation with passively measured solar induced fluorescence (SIF) and Eddy covariance (EC) carbon flux measurements can potentially lead to a novel PSII-GPP modeling framework to study salt marsh productivity at a higher spatio-temporal scale.